INTERNATIONAL JOURNAL FOR NUMERICAL METHODS IN ENGINEERING
Int. J. Numer. Meth. Engng 2003; **56**:2233–2266 (DOI: 10.1002/nme.662)

Geometrically non-linear anisotropic inelasticity based on fictitious configurations: Application to the coupling of continuum damage and multiplicative elasto-plasticity‡

A. Menzel and P. Steinmann*,†

Chair of Applied Mechanics, University of Kaiserslautern, Kaiserslautern, Germany

SUMMARY

The objective of this contribution is the formulation and algorithmic treatment of a phenomenological framework to capture anisotropic, geometrically non-linear inelasticity.

In addition to the intermediate configuration of multiplicative elasto-plasticity, we further introduce two microscopic configurations of Lagrangian and Eulerian type which characterize the so-called fictitious undamaged material. This kinematical framework enables us to apply two well-established postulates based on standard terminology in non-linear continuum mechanics. Concerning the free energy function, the postulate of strain energy equivalence is adopted and in view of the plastic dissipation potential the concept of effective stress is a natural outcome of the underlying kinematical assumptions.

Finally, we focus on the integration technique for the class of obtained evolution equations and present numerical examples for a prototype model to underline the applicability of the proposed framework.

KEY WORDS: anisotropy; fictitious configurations; continuum damage; multiplicative elasto-plasticity

1. INTRODUCTION

It is a desirable feature of a continuum damage theory to provide sufficient freedom to capture the anisotropic nature of damage. Thus the state of damage has to be described by at least a second order tensor, see Reference [1]. In this contribution, the underlying mechanism to incorporate the effects of damage is provided by the hypothesis of strain energy equivalence between microscopic and macroscopic configurations, see References [2–5]. The approach allows the interpretation as covariance of the free energy with respect to superposed diffeomorphisms, which are identified here with a damage deformation gradient. As

*Correspondence to: P. Steinmann, Lehrstuhl für Technische Mechanik, Universität Kaiserslautern, Erwin-Schrödinger-Strasse, Kaiserslautern D-67653, Germany.
†E-mail: ps@rhrk.uni-kl.de
‡Dedicated to the occasion of the 60th birthday of Professor Howard (Buck) L. Schreyer.

Contract/grant sponsor: Stiftung Rheinland-Pfalz für Innovation; contract/grant number: 8312-38 62 61/378

Received 5 November 2001
Revised 8 March 2002
Accepted 10 June 2002

an interesting aspect, the present damage metric based formulation may formally be related to the classical understanding of damage as an area reduction. Moreover, damage conditions formulated in the appropriate dissipative quantities and evolution laws for the damage metric and the internal variables are a natural outcome of the applied thermodynamically consistent framework. Thereby, the assumed dissipation potential essentially affects the type of damage evolution. In particular, we deal with initially anisotropic materials and deformation induced anisotropy.

Based on this idea, we develop a model formulation for anisotropic damage which is kinematically coupled to large inelastic deformations whereby the well-established framework of multiplicative elasto-plasticity is adopted, see e.g. References [6–11] references cited therein and the discussion by Naghdi [12]. For conceptual clarity, we restrict ourselves to the rate-independent case without loss of generality. In particular, the previously highlighted framework of Lagrangian fictitious, microscopic configurations is adopted which has until now been mainly used in continuum damage mechanics; see e.g. Brünig [13] for a similar approach. In this contribution, we relate elements of the tangent spaces of an undamaged, microscopic configuration and the standard intermediate configuration of multiplicative elasto-plasticity via a damage deformation gradient. Thereby, the previously mentioned covariance postulate is applied to the free energy function and the assumed damage dissipation potential. On top of this, a second fictitious configuration of Eulerian type is introduced and claimed to represent an isotropic setting with respect to the assumed plastic dissipation potential. Then, based on an essential kinematic assumption, the well-accepted concept of effective stress with respect to the construction of a yield function is a natural outcome of standard transformations in non-linear continuum mechanics, compare e.g. Reference [14].

The paper is organised as follows: To set the stage, the underlying kinematics related to the introduction of fictitious configurations are given in Section 2. Based on this, we set up the specific format of the free Helmholtz energy function, see Section 3. Later on, the theory of non-standard dissipative materials with application to multiplicative elasto-plasticity is highlighted in Section 4. Thereby, the incorporated Finger-type metric tensor in terms of a fictitious linear tangent map is treated as an internal variable and denoted as damage metric tensor. Section 5 deals with the construction of the incorporated dissipation potential. Finally, we focus on the integration of the obtained evolution equations—Section 6—and give some numerical examples in simple shear and a general finite element setting, see Section 7.

2. KINEMATICAL FRAMEWORK OF FICTITIOUS CONFIGURATIONS

For convenience of the reader, this section starts with a brief reiteration on essential kinematics of non-linear continuum mechanics and multiplicative elasto-plasticity. Based on this, we highlight the concept of fictitious configurations and introduce the applied notation. For more background information on non-linear kinematics in terms of convective co-ordinates, we refer to the works of Green and Zerna [15], Lodge [16] and Marsden and Hughes [17].

2.1. Notation for the overall motion

Let the material and spatial configuration of the considered body be denoted by $\mathscr{B}_0 \subset \mathbb{E}^3$ and $\mathscr{B}_t \subset \mathbb{E}^3$. The non-linear map of material points $\mathbf{X} \in \mathbb{V}^3$ onto spatial points $\mathbf{x}(\mathbf{X}, t) \in \mathbb{V}^3$ is

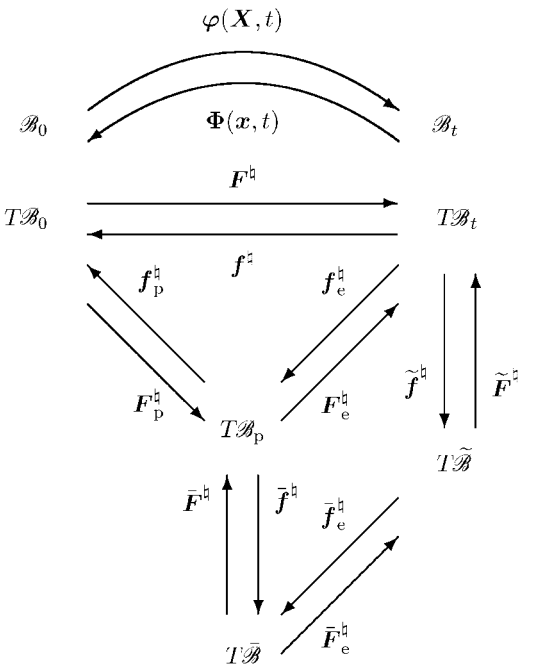

Figure 1. Non-linear point map $\boldsymbol{\varphi}$ and linear tangent maps $\mathbf{F}^\natural$, $\mathbf{F}^\natural_{\mathrm{p}}$, $\mathbf{F}^\natural_{\mathrm{e}}$, $\bar{\mathbf{F}}^\natural$, $\bar{\mathbf{F}}^\natural_{\mathrm{e}}$, $\tilde{\mathbf{F}}^\natural$.

represented by $\mathbf{x}=\boldsymbol{\varphi}(\mathbf{X},t)$ with $\boldsymbol{\varphi}(\mathbf{X},t):\mathscr{B}_0\times\mathbb{R}\to\mathscr{B}_t$, compare Figure 1. Thereby, let the denomination 'material point' allow the interpretation of a sufficiently large domain on the scale of the microstructure of the corresponding material. Next, referring to convected co-ordinates $\theta^i(\mathbf{x},t)$ and $\Theta^i(\mathbf{X})$, the natural and dual base vectors are characterized by the derivatives

$$\begin{aligned}\mathbf{g}_i &= \partial_{\theta^i}\mathbf{x}:T^*\mathscr{B}_t\to\mathbb{R}, \qquad \mathbf{g}^i = \partial_{\mathbf{x}}\theta^i:T\mathscr{B}_t\to\mathbb{R}\\ \mathbf{G}_i &= \partial_{\Theta^i}\mathbf{X}:T^*\mathscr{B}_0\to\mathbb{R}, \quad \mathbf{G}^i = \partial_{\mathbf{X}}\Theta^i:T\mathscr{B}_0\to\mathbb{R}\end{aligned} \tag{1}$$

and in addition, the spatial and material metric tensors are given as

$$\begin{aligned}\mathbf{g}^\flat &= g_{ij}\mathbf{g}^i\otimes\mathbf{g}^j:T\mathscr{B}_t\times T\mathscr{B}_t\to\mathbb{R}\\ \mathbf{g}^\sharp &= g^{ij}\mathbf{g}_i\otimes\mathbf{g}_j:T^*\mathscr{B}_t\times T^*\mathscr{B}_t\to\mathbb{R}\\ \mathbf{G}^\flat &= G_{ij}\mathbf{G}^i\otimes\mathbf{G}^j:T\mathscr{B}_0\times T\mathscr{B}_0\to\mathbb{R}\\ \mathbf{G}^\sharp &= G^{ij}\mathbf{G}_i\otimes\mathbf{G}_j:T^*\mathscr{B}_0\times T^*\mathscr{B}_0\to\mathbb{R}\end{aligned} \tag{2}$$

Moreover, we apply mixed-variant identity-tensors defined via

$$\mathbf{g}^\natural=\mathbf{g}_i\otimes\mathbf{g}^i:T\mathscr{B}_t\to T\mathscr{B}_t, \quad \mathbf{G}^\natural=\mathbf{G}_i\otimes\mathbf{G}^i:T\mathscr{B}_0\to T\mathscr{B}_0 \tag{3}$$

Then on a local chart, the linear tangent map of the direct motion is characterized by

$$\mathbf{F}^\natural(\mathbf{X},t)=\partial_{\mathbf{X}}\boldsymbol{\varphi}=\partial_{\theta^i}\boldsymbol{\varphi}\otimes\partial_{\mathbf{X}}\theta^i=\mathbf{g}_i\otimes\mathbf{G}^i\in:T\mathscr{B}_0\to T\mathscr{B}_t \tag{4}$$

with $\det \mathbf{F}^\natural \in \mathbb{R}_+$. For notational simplicity we introduce the corresponding linear tangent map of the inverse motion $\boldsymbol{\Phi}(\mathbf{x},t) = \boldsymbol{\varphi}^{-1} : \mathscr{B}_t \times \mathbb{R} \to \mathscr{B}_0$ via

$$\mathbf{f}^\natural(\mathbf{x},t) = \partial_{\mathbf{x}} \boldsymbol{\Phi} = \partial_{\Theta^i} \boldsymbol{\Phi} \otimes \partial_{\mathbf{x}} \Theta^i = \mathbf{G}_i \otimes \mathbf{g}^i : T\mathscr{B}_t \to T\mathscr{B}_0 \tag{5}$$

with $\det \mathbf{f}^\natural \in \mathbb{R}_+$ being obvious. Based on this, several kinematic tensors can be introduced like the right and left Cauchy–Green tensors (whereby we agree to the identification of the dual of the motion gradient with it's transposed)

$$\begin{aligned} \mathbf{C}^\flat &= \boldsymbol{\varphi}^* \mathbf{g}^\flat = [\mathbf{F}^\natural]^{\mathrm{t}} \cdot \mathbf{g}^\flat \cdot \mathbf{F}^\natural = g_{ij} \mathbf{G}^i \otimes \mathbf{G}^j \\ \mathbf{B}^\sharp &= \boldsymbol{\Phi}_* \mathbf{g}^\sharp = \mathbf{F}^\natural \cdot \mathbf{g}^\sharp \cdot [\mathbf{F}^\natural]^{\mathrm{t}} = g^{ij} \mathbf{G}_i \otimes \mathbf{G}_j \end{aligned} \tag{6}$$

which enter e.g. the definition of the Green–Lagrange strain tensor $\mathbf{E}^\flat = \frac{1}{2}[\mathbf{C}^\flat - \mathbf{G}^\flat]$.

2.2. Essential kinematics of multiplicative elasto-plasticity

Let the natural and dual tangent space of the intermediate configuration within multiplicative elasto-plasticity be denoted by $T\mathscr{B}_{\mathrm{p}}$ and $T^*\mathscr{B}_{\mathrm{p}}$, respectively. Similarly to Equation (1), the corresponding tangent and dual vectors read

$$\hat{\mathbf{G}}_i : T^*\mathscr{B}_{\mathrm{p}} \to \mathbb{R}, \quad \hat{\mathbf{G}}^i : T\mathscr{B}_{\mathrm{p}} \to \mathbb{R} \tag{7}$$

which are obviously not derivable from positions vectors since the intermediate configuration is generally incompatible. Consequently, the metric tensors and the identity in $\mathscr{B}_{\mathrm{p}}$ are given as

$$\begin{aligned} \hat{\mathbf{G}}^\flat &= \hat{G}_{ij} \hat{\mathbf{G}}^i \otimes \hat{\mathbf{G}}^j : T\mathscr{B}_{\mathrm{p}} \times T\mathscr{B}_{\mathrm{p}} \to \mathbb{R} \\ \hat{\mathbf{G}}^\sharp &= \hat{G}^{ij} \hat{\mathbf{G}}_i \otimes \hat{\mathbf{G}}_j : T^*\mathscr{B}_{\mathrm{p}} \times T^*\mathscr{B}_{\mathrm{p}} \to \mathbb{R} \\ \hat{\mathbf{G}}^\natural &= \hat{\mathbf{G}}_i \otimes \hat{\mathbf{G}}^i : T\mathscr{B}_{\mathrm{p}} \to T\mathscr{B}_{\mathrm{p}} \end{aligned} \tag{8}$$

It is then obvious that the elastic and plastic linear tangent maps which define the multiplicative decomposition of the deformation gradient with respect to the direct motion, $\mathbf{F}^\natural = \mathbf{F}_{\mathrm{e}}^\natural \cdot \mathbf{F}_{\mathrm{p}}^\natural$, are given by

$$\mathbf{F}_{\mathrm{p}}^\natural = \hat{\mathbf{G}}_i \otimes \mathbf{G}^i : T\mathscr{B}_0 \to T\mathscr{B}_{\mathrm{p}}, \quad \mathbf{F}_{\mathrm{e}}^\natural = \mathbf{g}_i \otimes \hat{\mathbf{G}}^i : T\mathscr{B}_{\mathrm{p}} \to T\mathscr{B}_t \tag{9}$$

and $\det \mathbf{F}_{\mathrm{p}}^\natural, \det \mathbf{F}_{\mathrm{e}}^\natural \in \mathbb{R}_+$. We now introduce in analogy to Equation (5),

$$\mathbf{f}_{\mathrm{p}}^\natural = \mathbf{G}_i \otimes \hat{\mathbf{G}}^i : T\mathscr{B}_{\mathrm{p}} \to T\mathscr{B}_0, \quad \mathbf{f}_{\mathrm{e}}^\natural = \hat{\mathbf{G}}_i \otimes \mathbf{g}^i : T\mathscr{B}_t \to T\mathscr{B}_{\mathrm{p}} \tag{10}$$

for the sake of notational simplicity with $\det \mathbf{f}_{\mathrm{p}}^\natural, \det \mathbf{f}_{\mathrm{e}}^\natural \in \mathbb{R}_+$ being obvious. Based on this setting, typical kinematic tensors can be constructed similar to Equations (6), namely

$$\begin{aligned} \hat{\mathbf{C}}_{\mathrm{e}}^\flat = \mathbf{F}_{\mathrm{e}}^\natural{}^\star \mathbf{g}^\flat = [\mathbf{F}_{\mathrm{e}}^\natural]^{\mathrm{t}} \cdot \mathbf{g}^\flat \cdot \mathbf{F}_{\mathrm{e}}^\natural &= g_{ij} \hat{\mathbf{G}}^i \otimes \hat{\mathbf{G}}^j \\ \hat{\mathbf{B}}_{\mathrm{e}}^\sharp = \mathbf{f}_{\mathrm{e}}^\natural{}_\star \mathbf{g}^\sharp = \mathbf{f}_{\mathrm{e}}^\natural \cdot \mathbf{g}^\sharp \cdot [\mathbf{f}_{\mathrm{e}}^\natural]^{\mathrm{t}} &= g^{ij} \hat{\mathbf{G}}_i \otimes \hat{\mathbf{G}}_j \end{aligned} \tag{11}$$

whereby, the notations $[\bullet]_\star$ and $[\bullet]^\star$ indicate pushforward and pullback operations, respectively. Furthermore, the elastic Green–Lagrange strain tensor with respect to the intermediate configuration is again obtained in standard format and reads $\hat{\mathbf{E}}_{\mathrm{e}}^\flat = \frac{1}{2}[\hat{\mathbf{C}}_{\mathrm{e}}^\flat - \hat{\mathbf{G}}^\flat]$.

2.3. Introduction of fictitious configurations

Next, on top of the spatial ($\mathscr{B}_t$), the intermediate ($\mathscr{B}_\mathrm{p}$) and the material ($\mathscr{B}_0$) configurations, we introduce additional fictitious configurations which are generally incompatible.

We first consider a fictitious or rather effective configuration which is assumed to be isotropic with respect to the free Helmholtz energy density and attached to the intermediate configuration of multiplicative elasto-plasticity. The corresponding tangent space and the dual space are denoted by $T\bar{\mathscr{B}}$ and $T^*\bar{\mathscr{B}}$, respectively. Consequently, the direct fictitious linear tangent map $\bar{\mathbf{F}}^\natural$ allows interpretation as an affine pre-deformation and defines the fictitious natural and dual base vectors

$$\bar{\mathbf{G}}_i : T^*\bar{\mathscr{B}} \to \mathbb{R}, \quad \bar{\mathbf{G}}^i : T\bar{\mathscr{B}} \to \mathbb{R} \tag{12}$$

which are again not derivable from position vectors. Continuing in this direction, we obtain fictitious metric tensors and the second order identity as

$$\begin{aligned} \bar{\mathbf{G}}^\flat &= \bar{G}_{ij}\bar{\mathbf{G}}^i \otimes \bar{\mathbf{G}}^j : T\bar{\mathscr{B}} \times T\bar{\mathscr{B}} \to \mathbb{R} \\ \bar{\mathbf{G}}^\sharp &= \bar{G}^{ij}\bar{\mathbf{G}}_i \otimes \bar{\mathbf{G}}_j : T^*\bar{\mathscr{B}} \times T^*\bar{\mathscr{B}} \to \mathbb{R} \\ \bar{\mathbf{G}}^\natural &= \bar{\mathbf{G}}_i \otimes \bar{\mathbf{G}}^i : T\bar{\mathscr{B}} \to T\bar{\mathscr{B}} \end{aligned} \tag{13}$$

Likewise, the linear tangent maps of the direct and inverse fictitious mapping follow straightforward

$$\bar{\mathbf{F}}^\natural = \hat{\mathbf{G}}_i \otimes \bar{\mathbf{G}}^i : T\bar{\mathscr{B}} \to T\mathscr{B}_\mathrm{p}, \quad \bar{\mathbf{f}}^\natural = \bar{\mathbf{G}}_i \otimes \hat{\mathbf{G}}^i : T\mathscr{B}_\mathrm{p} \to T\bar{\mathscr{B}} \tag{14}$$

with $\det \bar{\mathbf{F}}^\natural, \det \bar{\mathbf{f}}^\natural \in \mathbb{R}_+$ —see Figure 1 for a graphical representation.

Second, think of a fictitious or rather effective configuration which is isotropic with respect to an assumed plastic dissipation potential and also attached to the previously introduced fictitious configuration and to the spatial setting $\mathscr{B}_t$. The corresponding tangent space and the dual space are denoted by $T\tilde{\mathscr{B}}_0$ and $T^*\tilde{\mathscr{B}}_0$, respectively. Similar to Equation (12), we obtain fictitious natural and dual base vectors

$$\tilde{\mathbf{g}}_i : T^*\tilde{\mathscr{B}} \to \mathbb{R}, \quad \tilde{\mathbf{g}}^i : T\tilde{\mathscr{B}} \to \mathbb{R} \tag{15}$$

whereby again no interpretations as derivatives with respect to position vectors hold. The corresponding fictitious metric tensors and the second order identity consequently follow straightforward as

$$\begin{aligned} \tilde{\mathbf{g}}^\flat &= \tilde{g}_{ij}\tilde{\mathbf{g}}^i \otimes \tilde{\mathbf{g}}^j : T\tilde{\mathscr{B}} \times T\tilde{\mathscr{B}} \to \mathbb{R} \\ \tilde{\mathbf{g}}^\sharp &= \tilde{g}^{ij}\tilde{\mathbf{g}}_i \otimes \tilde{\mathbf{g}}_j : T^*\tilde{\mathscr{B}} \times T^*\tilde{\mathscr{B}} \to \mathbb{R} \\ \tilde{\mathbf{g}}^\natural &= \tilde{\mathbf{g}}_i \otimes \tilde{\mathbf{g}}^i : T\tilde{\mathscr{B}} \to T\tilde{\mathscr{B}} \end{aligned} \tag{16}$$

Likewise, the linear tangent maps of the direct and inverse fictitious mapping read as

$$\begin{aligned} \bar{\mathbf{F}}_\mathrm{e}^\natural &= \tilde{\mathbf{g}}_i \otimes \bar{\mathbf{G}}^i : T\bar{\mathscr{B}} \to T\tilde{\mathscr{B}}, \quad \bar{\mathbf{f}}_\mathrm{e}^\natural = \bar{\mathbf{G}}_i \otimes \tilde{\mathbf{g}}^i : T\tilde{\mathscr{B}} \to T\bar{\mathscr{B}} \\ \tilde{\mathbf{F}}^\natural &= \mathbf{g}_i \otimes \tilde{\mathbf{g}}^i : T\tilde{\mathscr{B}} \to T\mathscr{B}_t, \quad \tilde{\mathbf{f}}^\natural = \tilde{\mathbf{g}}_i \otimes \mathbf{g}^i : T\mathscr{B}_t \to T\tilde{\mathscr{B}} \end{aligned} \tag{17}$$

and $\det\bar{\mathbf{F}}_{\mathrm{e}}^{\natural}, \det\bar{\mathbf{f}}_{\mathrm{e}}^{\natural}, \det\tilde{\mathbf{F}}^{\natural}, \det\tilde{\mathbf{f}}^{\natural} \in \mathbb{R}_+$ —see again Figure 1 for a graphical representation. In particular, we end up with the useful relations

$$\tilde{\mathbf{F}}^{\natural} = \mathbf{F}_{\mathrm{e}}^{\natural} \cdot \bar{\mathbf{F}}^{\natural} \cdot \bar{\mathbf{f}}_{\mathrm{e}}^{\natural}, \quad \tilde{\mathbf{f}}^{\natural} = \bar{\mathbf{F}}_{\mathrm{e}}^{\natural} \cdot \bar{\mathbf{f}}^{\natural} \cdot \mathbf{f}_{\mathrm{e}}^{\natural} \tag{18}$$

3. CONSTRUCTION OF THE FREE ENERGY DENSITY

For the construction of the free Helmholtz energy density ψ_0^{p} with respect to the intermediate configuration, a contra-variant energy metric tensor (Finger-type) is introduced in the progression of this contribution which we denote by $\bar{\mathbf{A}}^{\sharp}$ and $\hat{\mathbf{A}}^{\sharp}$ with respect to the fictitious and the intermediate configuration, respectively. Thereby, the push-forward operation

$$\bar{\mathbf{F}}^{\natural} \star \bar{\mathbf{A}}^{\sharp} = \bar{\mathbf{F}}^{\natural} \cdot \bar{\mathbf{A}}^{\sharp} \cdot [\bar{\mathbf{F}}^{\natural}]^{\mathrm{t}} \doteq \hat{\mathbf{A}}^{\sharp} \tag{19}$$

is implied throughout. Now, as the key idea of this framework, the fictitious energy metric tensor is chosen to be equal to the fictitious contra-variant metric tensor, $\bar{\mathbf{A}}^{\sharp} \doteq \bar{\mathbf{G}}^{\sharp}$, and thus replaces this metric within the construction of the free Helmholtz energy density. Hence the fictitious configuration is isotropic and, remarkably, standard isotropic constitutive equations can be applied to model anisotropic material behaviour, e.g. in the intermediate configuration. Note that besides this specific choice, no further assumptions enter the proposed formulation. Isotropy is included in particular if the energy metric tensor $\hat{\mathbf{A}}^{\sharp}$ is a spherical tensor whereas otherwise anisotropy comes into the picture.

Next, to demonstrate the nature of this energy metric tensor, we choose a specific ansatz for the fictitious dual vectors $\bar{\mathbf{G}}^{i}$ with respect to the anisotropic intermediate configuration

$$\bar{\mathbf{G}}^{i} = [\bar{\mathbf{F}}^{\natural}]^{\mathrm{t}} \cdot \hat{\mathbf{G}}^{i} \doteq \alpha_0 \, \hat{\mathbf{G}}^{i} + \sum_{j=1}^{2} \alpha_j \, {}^{\hat{A}^{\sharp}}\hat{N}_j^{i} \, {}^{\hat{A}^{\flat}}\hat{\mathbf{N}}_j^{\flat} \tag{20}$$

whereby ${}^{\hat{A}^{\flat}}\hat{\mathbf{N}}_j^{\flat}$ are co-variant unit-vectors and ${}^{\hat{A}^{\sharp}}\hat{N}_j^{i} = \bar{\mathbf{G}}^{i} \cdot {}^{\hat{A}^{\sharp}}\hat{\mathbf{N}}_j^{\sharp}$ denote the components of their contra-variant complement. With these relations at hand, the two-point tensor $\bar{\mathbf{F}}^{\natural} = \hat{\mathbf{G}}_i \otimes \bar{\mathbf{G}}^{i}$ results in

$$\bar{\mathbf{F}}^{\natural} \doteq \alpha_0 \hat{\mathbf{G}}^{\natural} + \sum_{j=1}^{2} \alpha_j \hat{\mathbf{A}}_j^{\natural} \quad \text{with} \quad \hat{\mathbf{A}}_j^{\natural} = {}^{\hat{A}^{\sharp}}\hat{\mathbf{N}}_j^{\sharp} \otimes {}^{\hat{A}^{\flat}}\hat{\mathbf{N}}_j^{\flat} \tag{21}$$

For the restrictions on the scalars $\alpha_{0,1,2}$ in order to guarantee $\det\bar{\mathbf{F}}^{\natural} \in \mathbb{R}_+$, see Reference [18]. Consequently, straightforward computations based on Equation (19) and $\bar{\mathbf{A}}^{\sharp} \doteq \bar{\mathbf{G}}^{\sharp}$ render the symmetric energy metric tensor

$$\hat{\mathbf{A}}^{\sharp} = \beta_0 \hat{\mathbf{G}}^{\sharp} + \beta_1 \hat{\mathbf{A}}_1^{\sharp} + \beta_2 \hat{\mathbf{A}}_2^{\sharp} + 2\beta_3 [\hat{\mathbf{A}}_1^{\sharp} \cdot \hat{\mathbf{G}}^{\flat} \cdot \hat{\mathbf{A}}_2^{\sharp}]^{\mathrm{sym}} \tag{22}$$

whereby the abbreviated notations $\beta_0 = \alpha_0^2$, $\beta_1 = 2\alpha_0\alpha_1 + \alpha_1^2$, $\beta_2 = 2\alpha_0\alpha_2 + \alpha_2^2$, $\beta_3 = \alpha_1\alpha_2$ and the symmetry operation $[\bullet]_{ij}^{\mathrm{sym}} = \frac{1}{2}[[\bullet]_{ij} + [\bullet]_{ij}^{\mathrm{t}}] = \frac{1}{2}[[\bullet]_{ij} + [\bullet]_{ji}]$ (with respect to a Cartesian frame) have been introduced. Thereby, the rank one tensors $\hat{\mathbf{A}}_{1,2}^{\sharp}$ allow similar interpretations as structural tensors. Moreover, based on the spectral decomposition theorem of symmetric

second order tensors, the useful relation

$$\hat{\mathbf{A}}^{\sharp} = \sum_{i=1}^{3} {}^{\hat{A}^{\sharp}}\lambda_i \, {}^{\hat{A}^{\sharp}}\hat{\mathbf{N}}^{\sharp}_{i(\mathrm{spe})} \otimes {}^{\hat{A}^{\sharp}}\hat{\mathbf{N}}^{\sharp}_{i(\mathrm{spe})} = \eta_0 \hat{\mathbf{G}}^{\sharp} + \sum_{i=1}^{2} \eta_i \, {}^{\hat{A}^{\sharp}}\hat{\mathbf{N}}^{\sharp}_{i(\mathrm{spe})} \otimes {}^{\hat{A}^{\sharp}}\hat{\mathbf{N}}^{\sharp}_{i(\mathrm{spe})} \tag{23}$$

holds with ${}^{\hat{A}^{\sharp}}\lambda_i > 0$, $\eta_0 = {}^{\hat{A}^{\sharp}}\lambda_3$, $\eta_1 = {}^{\hat{A}^{\sharp}}\lambda_1 - {}^{\hat{A}^{\sharp}}\lambda_3$, $\eta_2 = {}^{\hat{A}^{\sharp}}\lambda_2 - {}^{\hat{A}^{\sharp}}\lambda_3$; compare Reference [19]. The representations (22) and (23) are obviously identical if $\beta_3 = 0$.

In the following, as the key idea of the proposed damage formulation, the energy metric tensor $\hat{\mathbf{A}}^{\sharp}$ is introduced as an internal variable which accounts for damage evolution and is thus denoted as damage metric tensor. Consequently, the fictitious linear tangent map $\bar{\mathbf{F}}^{\natural}$ no longer remains constant as degradation takes place and allows the interpretation as damage deformation gradient. Nevertheless, the fictitious configuration represented by $T\bar{\mathscr{B}}$, $T^{*}\bar{\mathscr{B}}$ as portrayed in Figure 1, persists isotropic and undamaged. On the contrary, the intermediate configuration, as well as the material and spatial settings $\mathscr{B}_0$ and $\mathscr{B}_t$, might be damaged and anisotropic.

In this context, we adopt the common ansatz of an additive decomposition of the free Helmholtz energy density into an elastic or rather damage contribution and an additional hardening term defined by a scalar-valued hardening variable κ, i.e. $\psi_0^{\mathrm{p}}(\hat{\mathbf{E}}^{\flat}_{\mathrm{e}}, \kappa; \hat{\mathbf{A}}^{\sharp}) \doteq {}^{\mathrm{dam}}\psi_0^{\mathrm{p}}(\hat{\mathbf{E}}^{\flat}_{\mathrm{e}}; \hat{\mathbf{A}}^{\sharp}) + {}^{\mathrm{har}}\psi_0(\kappa)$ in $\mathscr{B}_{\mathrm{p}}$. For the crucial relation between the intermediate and the attached fictitious configuration we obtain

$${}^{\mathrm{dam}}\bar{\psi}_0(\bar{\mathbf{E}}^{\flat}_{\mathrm{e}}; \bar{\mathbf{A}}^{\sharp}) + {}^{\mathrm{har}}\psi_0(\kappa) = {}^{\mathrm{dam}}\psi_0^{\mathrm{p}}(\hat{\mathbf{E}}^{\flat}_{\mathrm{e}}; \hat{\mathbf{A}}^{\sharp}) + {}^{\mathrm{har}}\psi_0(\kappa) \tag{24}$$

Conceptually speaking, the free Helmholtz energy density remains invariant under any (covariant) action of a non-singular linear tangent map, here $\bar{\mathbf{F}}^{\natural}$, whereby it is obvious that the considered elastic strain tensor transforms as

$$\bar{\mathbf{f}}^{\star}\bar{\mathbf{E}}^{\flat}_{\mathrm{e}} = [\bar{\mathbf{f}}^{\natural}]^{\mathrm{t}} \cdot \bar{\mathbf{E}}^{\flat}_{\mathrm{e}} \cdot \bar{\mathbf{f}}^{\natural} = \hat{\mathbf{E}}^{\flat}_{\mathrm{e}} \tag{25}$$

Since the fictitious configuration is assumed to be isotropic, three (basic) invariants in terms of $\bar{\mathbf{E}}^{\flat}_{\mathrm{e}}$ and $\bar{\mathbf{A}}^{\sharp}$ determine the elastic or rather damage contribution to the free Helmholtz energy density. Application of standard transformations as highlighted in Equations (19) and (25) render two corresponding sets of invariants

$${}^{\bar{E}^{\flat}_{\mathrm{e}}\bar{A}^{\sharp}}I_n = \bar{\mathbf{G}}^{\natural} : [\bar{\mathbf{E}}^{\flat}_{\mathrm{e}} \cdot \bar{\mathbf{A}}^{\sharp}]^n = \hat{\mathbf{G}}^{\natural} : [\hat{\mathbf{E}}^{\flat}_{\mathrm{e}} \cdot \hat{\mathbf{A}}^{\sharp}]^n = {}^{\hat{E}^{\flat}_{\mathrm{e}}\hat{A}^{\sharp}}I_n \tag{26}$$

with $n = 1, 2, 3$. These relations underline that we are practically dealing with the postulate of strain energy equivalence, see e.g. Reference [20]. Indeed, the incorporation of Equation (22) into Equation (26) yields a set of invariants which can be expressed as functions of the set of invariants for general orthotropy in terms of structural tensors as highlighted e.g. by Spencer [21]. A detailed discussion on the underlying restrictions is given in Reference [18]. For the geometrically linear case, it is straightforward to show that we essentially deal with a subclass of rhombic symmetry.

4. NON-STANDARD DISSIPATIVE MATERIALS

In this section, we apply the concept of non-standard dissipative materials. For a general overview of the underlying theory see e.g. References [22, 23] or [24] and references cited therein.

The local form of the isothermal Clausius–Duhem inequality reads with respect to the intermediate configuration

$$\mathscr{D}_0^{\mathrm{p}} = [\hat{\mathbf{M}}^{\natural}]^{\mathrm{t}} : \hat{\mathbf{L}}^{\natural} - \partial_{\hat{\mathbf{E}}_{\mathrm{e}}^{\flat}} \psi_0^{\mathrm{p}} : \mathrm{D}_t \hat{\mathbf{E}}_{\mathrm{e}}^{\flat} - \partial_{\hat{\mathbf{A}}^{\sharp}} \psi_0^{\mathrm{p}} : \mathrm{D}_t \hat{\mathbf{A}}^{\sharp} - \partial_{\kappa} \psi_0^{\mathrm{p}} \mathrm{D}_t \kappa \geqslant 0 \tag{27}$$

whereby the notation D_t denotes the material time derivative, $[\hat{\mathbf{M}}^{\natural}]^{\mathrm{t}}$ characterizes the Mandel tensor, i.e. the pull-back of the mixed-variant representation of the Kirchhoff stress $\hat{\mathbf{M}}^{\natural} = \mathbf{f}_{\mathrm{e}}^{\natural} \cdot \mathbf{m}^{\natural \mathrm{t}} \cdot \mathbf{F}_{\mathrm{e}}^{\natural}$ with $[\mathbf{m}^{\natural}]^{\mathrm{t}} = \mathbf{g}^{\flat} \cdot \boldsymbol{\tau}^{\sharp}$, and

$$\hat{\mathbf{L}}^{\natural} = \mathbf{f}_{\mathrm{e}}^{\natural} \cdot \mathbf{l}^{\natural} \cdot \mathbf{F}_{\mathrm{e}}^{\natural} = \mathbf{f}_{\mathrm{e}}^{\natural} \cdot \mathrm{D}_t \mathbf{F}_{\mathrm{e}}^{\natural} + \mathrm{D}_t \mathbf{F}_{\mathrm{p}}^{\natural} \cdot \mathbf{f}_{\mathrm{p}}^{\natural} = \hat{\mathbf{L}}_{\mathrm{e}}^{\natural} + \hat{\mathbf{L}}_{\mathrm{p}}^{\natural} \tag{28}$$

determines the mixed-variant pull-back of the spatial velocity gradient $\mathbf{l}^{\natural} = \mathrm{D}_t \mathbf{F}_{\mathrm{e}}^{\natural} \cdot \mathbf{f}_{\mathrm{e}}^{\natural} + \mathbf{F}_{\mathrm{e}}^{\natural} \cdot \mathrm{D}_t \mathbf{F}_{\mathrm{p}}^{\natural} \cdot \mathbf{f}_{\mathrm{p}}^{\natural} \cdot \mathbf{f}_{\mathrm{e}}^{\natural}$ with respect to the intermediate configuration. Now, by taking the relationship

$$2\mathrm{D}_t \hat{\mathbf{E}}_{\mathrm{e}}^{\flat} = \mathrm{D}_t [\mathbf{F}_{\mathrm{e}}^{\natural}]^{\mathrm{t}} \cdot \mathbf{g}^{\flat} \cdot \mathbf{F}_{\mathrm{e}}^{\natural} + [\mathbf{F}_{\mathrm{e}}^{\natural}]^{\mathrm{t}} \cdot \mathbf{g}^{\flat} \cdot \mathrm{D}_t \mathbf{F}_{\mathrm{e}}^{\natural} = [\hat{\mathbf{L}}_{\mathrm{e}}^{\natural}]^{\mathrm{t}} \cdot \hat{\mathbf{C}}_{\mathrm{e}}^{\flat} + \hat{\mathbf{C}}_{\mathrm{e}}^{\flat} \cdot \hat{\mathbf{L}}_{\mathrm{e}}^{\natural} = 2[\hat{\mathbf{C}}_{\mathrm{e}}^{\flat} \cdot \hat{\mathbf{L}}_{\mathrm{e}}^{\natural}]^{\mathrm{sym}} \tag{29}$$

into account, the dissipation inequality allows the representation

$$\begin{aligned} \mathscr{D}_0^{\mathrm{p}} &= [\hat{\mathbf{M}}^{\natural}]^{\mathrm{t}} : \hat{\mathbf{L}}^{\natural} - [\hat{\mathbf{C}}_{\mathrm{e}}^{\flat} \cdot \partial_{\hat{\mathbf{E}}_{\mathrm{e}}^{\flat}} \psi_0^{\mathrm{p}}] : \hat{\mathbf{L}}_{\mathrm{e}}^{\natural} - \partial_{\hat{\mathbf{A}}^{\sharp}} \psi_0^{\mathrm{p}} : \mathrm{D}_t \hat{\mathbf{A}}^{\sharp} - \partial_{\kappa} \psi_0^{\mathrm{p}} \mathrm{D}_t \kappa \\ &= [[\hat{\mathbf{M}}^{\natural}]^{\mathrm{t}} - \hat{\mathbf{C}}_{\mathrm{e}}^{\flat} \cdot \partial_{\hat{\mathbf{E}}_{\mathrm{e}}^{\flat}} \psi_0^{\mathrm{p}}] : \hat{\mathbf{L}}^{\natural} + [\hat{\mathbf{C}}_{\mathrm{e}}^{\flat} \cdot \partial_{\hat{\mathbf{E}}_{\mathrm{e}}^{\flat}} \psi_0^{\mathrm{p}}] : \hat{\mathbf{L}}_{\mathrm{p}}^{\natural} - \partial_{\hat{\mathbf{A}}^{\sharp}} \psi_0^{\mathrm{p}} : \mathrm{D}_t \hat{\mathbf{A}}^{\sharp} - \partial_{\kappa} \psi_0^{\mathrm{p}} \mathrm{D}_t \kappa \geqslant 0 \end{aligned} \tag{30}$$

Following the standard argumentation of rational thermodynamics, appropriate stress quantities are defined by

$$\begin{aligned} [\hat{\mathbf{M}}^{\natural}]^{\mathrm{t}} &\doteq \hat{\mathbf{C}}_{\mathrm{e}}^{\flat} \cdot \partial_{\hat{\mathbf{E}}_{\mathrm{e}}^{\flat}} \psi_0^{\mathrm{p}} \doteq \hat{\mathbf{C}}_{\mathrm{e}}^{\flat} \cdot \partial_{\hat{\mathbf{E}}_{\mathrm{e}}^{\flat}}{}^{\mathrm{dam}} \psi_0^{\mathrm{p}} \doteq \hat{\mathbf{C}}_{\mathrm{e}}^{\flat} \cdot \hat{\mathbf{S}}^{\sharp} \\ -\hat{\mathbf{Z}}^{\flat} &\doteq \partial_{\hat{\mathbf{A}}^{\sharp}} \psi_0^{\mathrm{p}} \doteq \partial_{\hat{\mathbf{A}}^{\sharp}}{}^{\mathrm{dam}} \psi_0^{\mathrm{p}} \\ -H &\doteq \partial_{\kappa} \psi_0^{\mathrm{p}} \doteq \partial_{\kappa}{}^{\mathrm{har}} \psi_0 \end{aligned} \tag{31}$$

Thereby, with respect to the representation of the basic invariants in Equation (26), the derivatives of the damage contribution of the free Helmholtz energy function ${}^{\mathrm{dam}}\psi_0^{\mathrm{p}} = {}^{\mathrm{dam}}\psi_0^{\mathrm{p}}(\hat{E}_{\mathrm{e}}^{\flat} \hat{A}^{\sharp} I_{1,2,3})$ take the following format

$$\begin{aligned} \hat{\mathbf{S}}^{\sharp} &= \sum_{n=1}^{3} n \partial_{\hat{E}_{\mathrm{e}}^{\flat} \hat{A}^{\sharp} I_n}{}^{\mathrm{dam}} \psi_0^{\mathrm{p}} \hat{\mathbf{A}}^{\sharp} \cdot [\hat{\mathbf{E}}_{\mathrm{e}}^{\flat} \cdot \hat{\mathbf{A}}^{\sharp}]^{[n-1]} \\ -\hat{\mathbf{Z}}^{\flat} &= \sum_{n=1}^{3} n \partial_{\hat{E}_{\mathrm{e}}^{\flat} \hat{A}^{\sharp} I_n}{}^{\mathrm{dam}} \psi_0^{\mathrm{p}} \hat{\mathbf{E}}_{\mathrm{e}}^{\flat} \cdot [\hat{\mathbf{A}}^{\sharp} \cdot \hat{\mathbf{E}}_{\mathrm{e}}^{\flat}]^{[n-1]} \end{aligned} \tag{32}$$

Now, with these definitions at hand, the reduced format of the isothermal dissipation inequality results in

$$^{\mathrm{red}}\mathscr{D}_0^{\mathrm{p}} = [\hat{\mathbf{M}}^{\natural}]^{\mathrm{t}} : \hat{\mathbf{L}}_{\mathrm{p}}^{\natural} + \hat{\mathbf{Z}}^{\flat} : \mathrm{D}_t \hat{\mathbf{A}}^{\sharp} + H \mathrm{D}_t \kappa = \hat{\mathbf{S}}^{\sharp} : \hat{\mathbf{D}}_{\mathrm{p}}^{\flat} + \hat{\mathbf{Z}}^{\flat} : \mathrm{D}_t \hat{\mathbf{A}}^{\sharp} + H \mathrm{D}_t \kappa \geqslant 0 \tag{33}$$

whereby the symmetric tensor $\hat{\mathbf{D}}_{\mathrm{p}}^{\flat} = [\hat{\mathbf{C}}_{\mathrm{e}}^{\flat} \cdot \hat{\mathbf{L}}_{\mathrm{p}}^{\natural}]^{\mathrm{sym}}$ has been introduced, compare Reference [25] with application to the more general framework based on an Eshelby stress tensor and $\det \mathbf{F}_{\mathrm{p}}^{\natural} \neq 1$. Note that $\hat{\mathbf{W}}_{\mathrm{p}}^{\flat} = [\hat{\mathbf{C}}_{\mathrm{e}}^{\flat} \cdot \hat{\mathbf{L}}_{\mathrm{p}}^{\natural}]^{\mathrm{skw}}$, which characterizes the plastic spin with respect to $\hat{\mathbf{C}}_{\mathrm{e}}^{\flat}$, is obviously undetermined within the representation in Equation (33).

Next, following the standard framework, we introduce an admissible elastic cone with respect to the intermediate configuration

$$\begin{aligned} \mathbb{A}^{\mathrm{p}} = \{([\hat{\mathbf{M}}^{\natural}]^{\mathrm{t}}, \bar{\mathbf{F}}^{\natural}, H; \hat{\mathbf{G}}^{\natural}) |\ & ^{\mathrm{yie}}\Phi^{\mathrm{p}}([\hat{\mathbf{M}}^{\natural}]^{\mathrm{t}}, \bar{\mathbf{F}}^{\natural}, H; \hat{\mathbf{G}}^{\natural}) \\ \doteq\ & ^{\mathrm{pla}}\Phi^{\mathrm{p}}([\hat{\mathbf{M}}^{\natural}]^{\mathrm{t}}, \bar{\mathbf{F}}^{\natural}; \hat{\mathbf{G}}^{\natural}) + {}^{\mathrm{har}}\Phi(H) \leqslant 0\} \end{aligned} \tag{34}$$

which is determined by the convex functions $^{\mathrm{pla}}\Phi^{\mathrm{p}}$ and $^{\mathrm{har}}\Phi$. Moreover, we assume the existence of a dissipation potential of Lemaitre-type, see e.g. Reference [14], namely

$$^{\mathrm{pot}}\Phi^{\mathrm{p}}([\hat{\mathbf{M}}^{\natural}]^{\mathrm{t}}, \bar{\mathbf{F}}^{\natural}, H, \hat{\mathbf{Z}}^{\flat}; \hat{\mathbf{G}}^{\natural}, \hat{\mathbf{A}}^{\sharp}) \doteq {}^{\mathrm{yie}}\Phi^{\mathrm{p}}([\hat{\mathbf{M}}^{\natural}]^{\mathrm{t}}, \bar{\mathbf{F}}^{\natural}, H; \hat{\mathbf{G}}^{\natural}) + {}^{\mathrm{dam}}\Phi^{\mathrm{p}}(\hat{\mathbf{Z}}^{\flat}; \hat{\mathbf{A}}^{\sharp}) \tag{35}$$

which will be specified in Section 5. In this context, appropriate evolution equations allow e.g. the following representation

$$\begin{aligned} \hat{\mathbf{L}}_{\mathrm{p}}^{\natural} &= \mathrm{D}_t \lambda \partial_{[\hat{\mathbf{M}}^{\natural}]^{\mathrm{t}}} {}^{\mathrm{pot}}\Phi^{\mathrm{p}} &&= \mathrm{D}_t \lambda \partial_{[\hat{\mathbf{M}}^{\natural}]^{\mathrm{t}}} {}^{\mathrm{pla}}\Phi^{\mathrm{p}} \\ \mathrm{D}_t \hat{\mathbf{A}}^{\sharp} &= \mathrm{D}_t \lambda \partial_{\hat{\mathbf{Z}}^{\flat}} {}^{\mathrm{pot}}\Phi^{\mathrm{p}} &&= \mathrm{D}_t \lambda \partial_{\hat{\mathbf{Z}}^{\flat}} {}^{\mathrm{dam}}\Phi^{\mathrm{p}} \\ \mathrm{D}_t \kappa &= \mathrm{D}_t \lambda \partial_H {}^{\mathrm{pot}}\Phi^{\mathrm{p}} &&= \mathrm{D}_t \lambda \partial_H {}^{\mathrm{har}}\Phi \end{aligned} \tag{36}$$

Obviously, we deal with associated evolution equations for the plasticity and hardening contributions but the damage part, nevertheless, remains non-associated.

Remark 4.1

Recall that, in view of Equation (33), an alternative format of an associated evolution equation for $\hat{\mathbf{L}}_{\mathrm{p}}^{\natural}$ can be introduced via

$$\begin{aligned} \hat{\mathbf{D}}_{\mathrm{p}}^{\flat} &= \mathrm{D}_t \lambda \partial_{\hat{\mathbf{S}}^{\sharp}} {}^{\mathrm{pla}}\Phi^{\mathrm{p}} = \mathrm{D}_t \lambda \partial_{[\hat{\mathbf{M}}^{\natural}]^{\mathrm{t}}} {}^{\mathrm{pla}}\Phi^{\mathrm{p}} : \partial_{\hat{\mathbf{S}}^{\sharp}} [\hat{\mathbf{C}}_{\mathrm{e}}^{\flat} \cdot \hat{\mathbf{S}}^{\sharp}] \\ &= \mathrm{D}_t \lambda \partial_{[\hat{\mathbf{M}}^{\natural}]^{\mathrm{t}}} {}^{\mathrm{pla}}\Phi^{\mathrm{p}} : \tfrac{1}{2} [\hat{\mathbf{C}}_{\mathrm{e}}^{\flat} \bar{\otimes} \hat{\mathbf{G}}^{\natural} + \hat{\mathbf{C}}_{\mathrm{e}}^{\flat} \underline{\otimes} \hat{\mathbf{G}}^{\natural}] \\ &= \mathrm{D}_t \lambda [\hat{\mathbf{C}}_{\mathrm{e}}^{\flat} \cdot \partial_{[\hat{\mathbf{M}}^{\natural}]^{\mathrm{t}}} {}^{\mathrm{pla}}\Phi^{\mathrm{p}}]^{\mathrm{sym}} \end{aligned} \tag{37}$$

compare Reference [26] and Equation (A4) for the definition of the non-standard dyadic products.

5. CONSTRUCTION OF THE INELASTIC POTENTIALS

In this section we discuss the construction of the inelastic potentials. Thereby, we choose different approaches concerning each single contribution. For the damage part, we apply the fundamental covariance postulate with respect to the intermediate and the Lagrangian fictitious configuration. Concerning the scalar-valued hardening contribution, well-established constitutive equations are adopted. Finally, a specific kinematic assumption is incorporated for the plasticity framework, which enables us to essentially deal with the postulate of effective stress.

5.1. Construction of the damage potential

The choice of the assumed damage potential significantly affects the evolution of damage and the anisotropic character of the material. Recall that we reiterate here a specific case of the most general framework defined by general, e.g. isotropic, tensor functions in terms of $\hat{\mathbf{Z}}^{\flat}$ and $\hat{\mathbf{A}}^{\sharp}$, compare Reference [27].

For the damage contribution ${}^{\mathrm{dam}}\Phi^{\mathrm{p}}(\hat{\mathbf{Z}}^{\flat};\hat{\mathbf{A}}^{\sharp})$, see Equation (35), we once more consider the fundamental covariance postulate in analogy to the free Helmholtz energy density. It obviously turns out that, similar to Equation (26), we again deal with only three invariants ($n=1,2,3$) which determine ${}^{\mathrm{dam}}\Phi^{\mathrm{p}}$

$$ {}^{\bar{Z}^{\flat}\bar{A}^{\sharp}}I_n = \bar{\mathbf{G}}^{\natural} : [\bar{\mathbf{Z}}^{\flat} \cdot \bar{\mathbf{A}}^{\sharp}]^n = \hat{\mathbf{G}}^{\natural} : [\hat{\mathbf{Z}}^{\flat} \cdot \hat{\mathbf{A}}^{\sharp}]^n = {}^{\hat{Z}^{\flat}\hat{A}^{\sharp}}I_n \tag{38} $$

since the fictitious configuration is isotropic with respect to the damage potential, $\bar{\mathbf{A}}^{\sharp} \doteq \bar{\mathbf{G}}^{\sharp}$. Based on this assumption, the general form of the dissipation potential reads as

$$ {}^{\mathrm{dam}}\Phi^{\mathrm{p}}(\hat{\mathbf{Z}}^{\flat};\hat{\mathbf{A}}^{\sharp}) = {}^{\mathrm{dam}}\Phi^{\mathrm{p}}({}^{\hat{Z}^{\flat}\hat{A}^{\sharp}}I_{1,2,3}) \tag{39} $$

5.1.1. Prototype models. Two specific representations seem to be natural and will be highlighted in the progression of this contribution, compare Reference [28].

The direct formulation introduces the damage rate coaxial to a symmetric, positive semi-definite second order tensor $\hat{\boldsymbol{\Xi}}^{\sharp}(\hat{\mathbf{A}}^{\sharp})$. Obviously, the simplest choice $\hat{\boldsymbol{\Xi}}^{\sharp} \doteq \hat{\mathbf{A}}^{\sharp}$ is based on the introduction of the first damage stress invariant ($\delta_1 \in \mathbb{R}_+$)

$$ \begin{aligned} {}^{\mathrm{dam}}\Phi^{\mathrm{p}}_{\mathrm{fix}} &\doteq \tfrac{1}{2}\,\delta_1\,{}^{\hat{Z}^{\flat}\hat{A}^{\sharp}}I_1^2 = \tfrac{1}{2}\,\delta_1[\hat{\mathbf{Z}}^{\flat} : \hat{\mathbf{A}}^{\sharp}]^2 \\ \Rightarrow \mathrm{D}_t\hat{\mathbf{A}}^{\sharp} &= \mathrm{D}_t\lambda\delta_1[\hat{\mathbf{Z}}^{\flat} : \hat{\mathbf{A}}^{\sharp}]\hat{\mathbf{A}}^{\sharp} \end{aligned} \tag{40} $$

Please note that the damage rate and the damage metric itself are coaxial. Nevertheless, since the damage metric could be non-spherical, we denote this type of damage evolution as *quasi isotropic*.

The formulation based on conjugate variables constructs the damage rate as a linear map of the damage stress via a symmetric, positive semi-definite fourth order tensor $\hat{\boldsymbol{\Xi}}^{\sharp}(\hat{\mathbf{A}}^{\sharp})$. Then the simple choice $\hat{\boldsymbol{\Xi}}^{\sharp} \propto \hat{\mathbf{A}}^{\sharp} \bar{\otimes} \hat{\mathbf{A}}^{\sharp}$ ends up with a quadratic form being proportional to the second damage stress invariant ($\delta_2 \in \mathbb{R}_+$)

$$\begin{aligned} {}^{\text{dam}}\Phi^{\text{p}}_{\text{cha}} &\doteq \tfrac{1}{2}\,\delta_2\, {}^{\hat{Z}^{\flat}\hat{A}^{\sharp}}I_2 = \tfrac{1}{2}\,\delta_2 \hat{\mathbf{Z}}^{\flat} : [\hat{\mathbf{A}}^{\sharp} \bar{\otimes} \hat{\mathbf{A}}^{\sharp}] : \hat{\mathbf{Z}}^{\flat} \\ \Rightarrow \mathrm{D}_t \hat{\mathbf{A}}^{\sharp} &= \mathrm{D}_t \lambda \delta_2 \hat{\mathbf{A}}^{\sharp} \cdot \hat{\mathbf{Z}}^{\flat} \cdot \hat{\mathbf{A}}^{\sharp} \end{aligned} \tag{41}$$

see Equation (A4) for the definition of the non-standard dyadic product. Now, the damage rate and the damage metric no longer commute which motivates the terminology *anisotropic damage*.

Obviously, these two types of damage functions in connection with the property of the initial damage metric tensor $\hat{\mathbf{A}}^{\sharp}|_{t_0}$ define a general classification of the coupling of hyperelasticity and damage. Naturally, there are four different categories which account for initial and deformation induced anisotropy, see Reference [29]. Please note that if we assume $\hat{\mathbf{A}}^{\sharp}|_{t_0} = \beta_0 \hat{\mathbf{G}}^{\sharp}$ within a linear St. Venant–Kirchhoff material and quasi isotropic damage evolution, this category is directly related to the classical isotropic $[1-D]$ damage formulation via $\hat{\mathbf{A}}^{\sharp} = \beta_0 \hat{\mathbf{G}}^{\sharp} = [1-D]\hat{\mathbf{G}}^{\sharp}$. Then β_0 no longer remains constant but rather characterizes three identical eigenvalues ${}^{\hat{A}^{\sharp}}\lambda_{1,2,3}$ which degrade for increasing damage. Moreover, recall that by starting with an initially isotropic material but taking anisotropic damage evolution into account, we may end up with anisotropic behaviour in the elastic domain for unloading after damage evolution has taken place.

5.2. Construction of the hardening potential

In the sequel, we adopt a well-established format for the proportional hardening potential, namely

$${}^{\text{har}}\Phi \doteq -\tfrac{1}{3}[Y_0 - H]^2 \tag{42}$$

with $Y_0 \in \mathbb{R}_+$, which results within the associated framework in the flow rule

$$\mathrm{D}_t \kappa = \mathrm{D}_t \lambda\, \tfrac{2}{3}[Y_0 - H] \tag{43}$$

5.3. Construction of the plastic potential

Next, for the definition of the invariants which enter the plastic contribution of the dissipation potential, we assume the Eulerian fictitious tangent space $T\tilde{\mathscr{B}}$ to represent an isotropic configuration. Now, similar to $\bar{\mathbf{A}}^{\sharp}$ within the damage formulation, $\tilde{\mathbf{p}}^{\flat}$ denotes a co-variant dissipation metric. In the following, $\tilde{\mathbf{p}}^{\flat} \doteq \tilde{\mathbf{g}}^{\flat}$ is assumed throughout and we thus define an isotropic configuration for

$${}^{\text{pla}}\tilde{\Phi} = {}^{\text{pla}}\tilde{\Phi}(\tilde{\boldsymbol{\tau}}^{\sharp}; \tilde{\mathbf{p}}^{\flat}) \doteq {}^{\text{pla}}\tilde{\Phi}(\tilde{\boldsymbol{\tau}}^{\sharp}; \tilde{\mathbf{g}}^{\flat}) \tag{44}$$

whereby $\tilde{\boldsymbol{\tau}}^{\sharp} = \tilde{\mathbf{f}}^{\natural} \star \boldsymbol{\tau}^{\sharp}$ represents the pull-back to $T\tilde{\mathscr{B}}$ of the Kirchhoff stress tensor in $\mathscr{B}_t$. Now, standard transformations yield the plastic potential with respect to the intermediate configuration

$${}^{\text{pla}}\tilde{\Phi} = {}^{\text{pla}}\tilde{\Phi}(\bar{\mathbf{F}}^{\natural} \star \bar{\mathbf{f}}^{\natural}_{\text{e}} \star \tilde{\boldsymbol{\tau}}^{\sharp}; \bar{\mathbf{f}}^{\natural} \star \bar{\mathbf{F}}^{\natural}_{\text{e}} \star \tilde{\mathbf{p}}^{\flat}) = {}^{\text{pla}}\bar{\Phi}(\bar{\mathbf{F}}^{\natural} \star \bar{\mathbf{S}}^{\sharp}; \bar{\mathbf{f}}^{\natural} \star \bar{\mathbf{P}}^{\flat}) = {}^{\text{pla}}\Phi^{\text{p}}(\hat{\mathbf{S}}^{\sharp}; \hat{\mathbf{P}}^{\flat}) \tag{45}$$

Please note that $\hat{\mathbf{S}}^{\sharp} = \bar{\mathbf{F}}^{\natural} \star \bar{\mathbf{f}}_{\mathrm{e}}^{\natural} \star \tilde{\mathbf{f}}_{\mathrm{e}}^{\natural} \star \boldsymbol{\tau}^{\sharp} = \mathbf{f}_{\mathrm{e}}^{\natural} \star \boldsymbol{\tau}^{\sharp}$ denotes the pull-back of the Kirchhoff stress to the intermediate configuration. Based on this, we make the key assumption of the proposed plasticity framework, namely that the fictitious elastic linear tangent map $\bar{\mathbf{F}}_{\mathrm{e}}^{\natural}$ equals the elastic linear tangent map $\mathbf{F}_{\mathrm{e}}^{\natural}$ of the multiplicative decomposition. Consequently, in view of the involved Cauchy–Green-type tensors, we obtain the crucial relationship

$$\bar{\mathbf{F}}_{\mathrm{e}}^{\natural} \doteq \mathbf{F}_{\mathrm{e}}^{\natural} \Rightarrow \bar{\mathbf{P}}^{\flat} = \bar{\mathbf{F}}_{\mathrm{e}}^{\natural} \star \tilde{\mathbf{p}}^{\flat} = [\bar{\mathbf{F}}_{\mathrm{e}}^{\natural}]^{\mathrm{t}} \cdot \tilde{\mathbf{p}}^{\flat} \cdot \bar{\mathbf{F}}_{\mathrm{e}}^{\natural} \equiv \mathbf{F}_{\mathrm{e}}^{\natural} \star \mathbf{g}^{\flat} = [\mathbf{F}_{\mathrm{e}}^{\natural}]^{\mathrm{t}} \cdot \mathbf{g}^{\flat} \cdot \mathbf{F}_{\mathrm{e}}^{\natural} = \hat{\mathbf{C}}_{\mathrm{e}}^{\flat} \tag{46}$$

based on $\tilde{\mathbf{p}}^{\flat} \doteq \tilde{\mathbf{g}}^{\flat}$. In this direction, the plastic part of the yield function with respect to the intermediate configuration results in

$$\begin{aligned}
{}^{\mathrm{pla}}\tilde{\Phi}(\tilde{\boldsymbol{\tau}}^{\sharp}; \tilde{\mathbf{p}}^{\flat}) &= {}^{\mathrm{pla}}\tilde{\Phi}(\bar{\mathbf{F}}^{\natural} \star \bar{\mathbf{f}}_{\mathrm{e}}^{\natural} \star \tilde{\boldsymbol{\tau}}^{\sharp}; \bar{\mathbf{f}}^{\natural} \star \bar{\mathbf{F}}_{\mathrm{e}}^{\natural} \star \tilde{\mathbf{p}}^{\flat}) = {}^{\mathrm{pla}}\Phi^{\mathrm{p}}(\hat{\mathbf{S}}^{\sharp}; \bar{\mathbf{f}}^{\natural} \star \bar{\mathbf{P}}^{\flat}) \\
&\equiv {}^{\mathrm{pla}}\Phi^{\mathrm{p}}(\hat{\mathbf{S}}^{\sharp}; \bar{\mathbf{f}}^{\natural} \star \hat{\mathbf{C}}_{\mathrm{e}}^{\flat}) = {}^{\mathrm{pla}}\Phi^{\mathrm{p}}(\bar{\mathbf{f}}^{\natural} \star \hat{\mathbf{C}}_{\mathrm{e}}^{\flat} \cdot \hat{\mathbf{S}}^{\sharp}; \hat{\mathbf{G}}^{\natural}) \\
&= {}^{\mathrm{pla}}\Phi^{\mathrm{p}}([\hat{\mathbf{M}}_{\mathrm{d}}^{\natural}]^{\mathrm{t}}; \hat{\mathbf{G}}^{\natural}) = {}^{\mathrm{pla}}\Phi^{\mathrm{p}}([\hat{\mathbf{M}}^{\natural}]^{\mathrm{t}}, \bar{\mathbf{F}}^{\natural}; \hat{\mathbf{G}}^{\natural})
\end{aligned} \tag{47}$$

with the modified Mandel stress $[\hat{\mathbf{M}}_{\mathrm{d}}^{\natural}]^{\mathrm{t}} \equiv \bar{\mathbf{f}}^{\natural} \star \hat{\mathbf{C}}_{\mathrm{e}}^{\flat} \cdot \hat{\mathbf{S}}^{\sharp}$. Thereby the fundamental covariance postulate has been applied and an appropriate set of invariants is given by

$$\begin{aligned}
{}^{\tilde{p}^{\flat}\tilde{\tau}^{\sharp}}I_n &= \tilde{\mathbf{g}}^{\natural} : [\tilde{\mathbf{p}}^{\flat} \cdot \tilde{\boldsymbol{\tau}}^{\sharp}]^n \\
&= \bar{\mathbf{G}}^{\natural} : [\bar{\mathbf{P}}^{\flat} \cdot \bar{\mathbf{S}}^{\sharp}]^n = {}^{\bar{P}^{\flat}\bar{S}^{\sharp}}I_n \\
&\equiv \hat{\mathbf{G}}^{\natural} : [\bar{\mathbf{f}}^{\natural} \star \hat{\mathbf{C}}_{\mathrm{e}}^{\flat} \cdot \hat{\mathbf{S}}^{\sharp}]^n = {}^{\bar{f}^{\natural} \star \hat{C}_{\mathrm{e}}^{\flat} \hat{S}^{\sharp}}I_n \\
&= \hat{\mathbf{G}}^{\natural} : [\hat{\mathbf{C}}_{\mathrm{e}}^{\flat} \cdot \bar{\mathbf{f}}^{\natural} \star \hat{\mathbf{S}}^{\sharp}]^n = {}^{\hat{C}_{\mathrm{e}}^{\flat} \bar{f}^{\natural} \star \hat{S}^{\sharp}}I_n \\
&\equiv \hat{\mathbf{G}}^{\natural} : [[\hat{\mathbf{M}}_{\mathrm{d}}^{\natural}]^{\mathrm{t}}]^n = {}^{\hat{G}^{\natural}[\hat{M}_{\mathrm{d}}^{\natural}]^{\mathrm{t}}}I_n
\end{aligned} \tag{48}$$

for $n = 1, 2, 3$. Note that in contrast to the free Helmholtz energy density and the damage potential, the linear tangent map $\bar{\mathbf{F}}^{\natural}$ explicitly enters the yield function. Pausing for a moment, we see that this is obviously a nice feature since the introduction of a damage spin within the coupling to plasticity is possible. Note that the set of invariants allows the representations

$$\begin{aligned}
{}^{\bar{f}^{\natural} \star \hat{C}_{\mathrm{e}}^{\flat} \hat{S}^{\sharp}}I_n &= \hat{\mathbf{G}}^{\natural} : [\hat{\mathbf{C}}_{\mathrm{e}[\bar{f}^{\natural}]^{\mathrm{t}}}^{\flat} \cdot \hat{\mathbf{S}}^{\sharp}]^n = {}^{\hat{C}_{\mathrm{e}[\bar{f}^{\natural}]^{\mathrm{t}}}^{\flat} \hat{S}^{\sharp}}I_n \\
{}^{\hat{C}_{\mathrm{e}}^{\flat} \bar{f}^{\natural} \star \hat{S}^{\sharp}}I_n &= \hat{\mathbf{G}}^{\natural} : [\hat{\mathbf{C}}_{\mathrm{e}}^{\flat} \cdot \hat{\mathbf{S}}_{\bar{f}^{\natural}}^{\sharp}]^n = {}^{\hat{C}_{\mathrm{e}}^{\flat} \hat{S}_{\bar{f}^{\natural}}^{\sharp}}I_n \\
{}^{\hat{G}^{\natural}[\hat{M}_{\mathrm{d}}^{\natural}]^{\mathrm{t}}}I_n &= \hat{\mathbf{G}}^{\natural} : [\hat{\mathbf{C}}_{\mathrm{e}[\bar{f}^{\natural}]^{\mathrm{t}}}^{\flat} \cdot \hat{\mathbf{S}}^{\sharp}]^n = \hat{\mathbf{G}}^{\natural} : [\hat{\mathbf{C}}_{\mathrm{e}}^{\flat} \cdot \hat{\mathbf{S}}_{\bar{f}^{\natural}}^{\sharp}]^n \\
\text{with} \quad \hat{\mathbf{C}}_{\mathrm{e}[\bar{f}^{\natural}]^{\mathrm{t}}}^{\flat} &= [[\bar{\mathbf{f}}^{\natural}]^{\mathrm{t}} \bar{\otimes} [\bar{\mathbf{f}}^{\natural}]^{\mathrm{t}}] : \hat{\mathbf{C}}_{\mathrm{e}}^{\flat} \\
\text{and} \quad \hat{\mathbf{S}}_{\bar{f}^{\natural}}^{\sharp} &= [\bar{\mathbf{f}}^{\natural} \bar{\otimes} \bar{\mathbf{f}}^{\natural}] : \hat{\mathbf{S}}^{\sharp}
\end{aligned} \tag{49}$$

for $n=1,2,3$, which underlines that the modified Mandel stress tensor $[\hat{\mathbf{M}}_{\mathrm{d}}^{\natural}]^{\mathrm{t}} \equiv \hat{\mathbf{C}}^{\flat}_{\mathrm{e}[\,\bar{f}^{\natural}]^{\mathrm{t}}} \cdot \hat{\mathbf{S}}^{\sharp}$ entering the plastic part of the yield function, is essentially obtained by a linear map of $\hat{\mathbf{C}}_{\mathrm{e}}^{\flat}$ via the fourth order tensor $[\bar{\mathbf{f}}^{\natural}]^{\mathrm{t}} \bar{\otimes} [\bar{\mathbf{f}}^{\natural}]^{\mathrm{t}}$ which accounts for anisotropy and degradation. Conceptually speaking, the appropriate metric tensor, with respect to the intermediate configuration, is modified such that anisotropy and degradation are incorporated into the yield function. Alternatively, a modified or rather effective stress tensor can be introduced to construct the appropriate set of invariants which is then determined by the linear mapping of $\hat{\mathbf{S}}^{\sharp}$ under the action of $\bar{\mathbf{f}}^{\natural} \bar{\otimes} \bar{\mathbf{f}}^{\natural}$. Then, referring to the Lagrangian fictitious configuration, we deal with the well-accepted concept of effective stress for the construction of the plastic potential.

Next, in view of Equation $(36)_1$, the corresponding associated evolution equation is given as

$$\begin{aligned}
\hat{\mathbf{L}}_{\mathrm{p}}^{\natural} &= \mathrm{D}_t \lambda \partial_{[\hat{\mathbf{M}}^{\natural}]^{\mathrm{t}}}{}^{\mathrm{pot}}\Phi^{\mathrm{p}} = \mathrm{D}_t \lambda \partial_{[\hat{\mathbf{M}}_{\mathrm{d}}^{\natural}]^{\mathrm{t}}}{}^{\mathrm{pla}}\Phi^{\mathrm{p}} : \partial_{\hat{\mathbf{S}}^{\sharp}}[\hat{\mathbf{M}}_{\mathrm{d}}^{\natural}]^{\mathrm{t}} : \partial_{[\hat{\mathbf{M}}^{\natural}]^{\mathrm{t}}}\hat{\mathbf{S}}^{\sharp} \\
&= \mathrm{D}_t \lambda \partial_{[\hat{\mathbf{M}}_{\mathrm{d}}^{\natural}]^{\mathrm{t}}}{}^{\mathrm{pla}}\Phi^{\mathrm{p}} : \tfrac{1}{2}[[\hat{\mathbf{C}}^{\flat}_{\mathrm{e}[\,\bar{f}^{\natural}]^{\mathrm{t}}} \cdot \hat{\mathbf{B}}_{\mathrm{e}}^{\sharp}] \bar{\otimes} \hat{\mathbf{G}}^{\natural} + \hat{\mathbf{C}}^{\flat}_{\mathrm{e}[\,\bar{f}^{\natural}]^{\mathrm{t}}} \underline{\otimes} \hat{\mathbf{B}}_{\mathrm{e}}^{\sharp}] \\
\text{with} \quad \partial_{\hat{\mathbf{S}}^{\sharp}}[\hat{\mathbf{M}}_{\mathrm{d}}^{\natural}]^{\mathrm{t}} &= \tfrac{1}{2}[\hat{\mathbf{C}}^{\flat}_{\mathrm{e}[\,\bar{f}^{\natural}]^{\mathrm{t}}} \bar{\otimes} \hat{\mathbf{G}}^{\natural} + \hat{\mathbf{C}}^{\flat}_{\mathrm{e}[\,\bar{f}^{\natural}]^{\mathrm{t}}} \underline{\otimes} \hat{\mathbf{G}}^{\natural}] \\
\text{and} \quad \partial_{[\hat{\mathbf{M}}^{\natural}]^{\mathrm{t}}}\hat{\mathbf{S}}^{\sharp} &= \hat{\mathbf{B}}_{\mathrm{e}}^{\sharp} \bar{\otimes} \hat{\mathbf{G}}^{\natural}
\end{aligned} \tag{50}$$

whereby the applied relation $\hat{\mathbf{B}}_{\mathrm{e}}^{\sharp} = [\hat{\mathbf{C}}_{\mathrm{e}}^{\flat}]^{-1}$ has been introduced in Equation $(11)_2$. Summarizing, we obtain the more compact format

$$\begin{aligned}
\hat{\mathbf{L}}_{\mathrm{p}}^{\natural} &= \mathrm{D}_t \lambda \tfrac{1}{2}[\hat{\mathbf{B}}_{\mathrm{e}}^{\sharp} \cdot \hat{\mathbf{C}}^{\flat}_{\mathrm{e}[\,\bar{f}^{\natural}]^{\mathrm{t}}} \cdot \partial_{[\hat{\mathbf{M}}_{\mathrm{d}}^{\natural}]^{\mathrm{t}}}{}^{\mathrm{pla}}\Phi^{\mathrm{p}} + \hat{\mathbf{B}}_{\mathrm{e}}^{\sharp} \cdot [\partial_{[\hat{\mathbf{M}}_{\mathrm{d}}^{\natural}]^{\mathrm{t}}}{}^{\mathrm{pla}}\Phi^{\mathrm{p}}]^{\mathrm{t}} \cdot \hat{\mathbf{C}}^{\flat}_{\mathrm{e}[\,\bar{f}^{\natural}]^{\mathrm{t}}}] \\
&= \mathrm{D}_t \lambda [\hat{\mathbf{B}}_{\mathrm{e}}^{\sharp} \cdot [\hat{\mathbf{C}}^{\flat}_{\mathrm{e}[\,\bar{f}^{\natural}]^{\mathrm{t}}} \cdot \partial_{[\hat{\mathbf{M}}_{\mathrm{d}}^{\natural}]^{\mathrm{t}}}{}^{\mathrm{pla}}\Phi^{\mathrm{p}}]^{\mathrm{sym}}] \\
&\doteq \mathrm{D}_t \lambda \hat{\mathbf{N}}^{\natural}_{\bar{f}^{\natural}}(\hat{\mathbf{N}}_{\mathrm{d}}^{\natural}, \hat{\mathbf{C}}^{\flat}_{\mathrm{e}[\,\bar{f}^{\natural}]^{\mathrm{t}}}, \hat{\mathbf{B}}_{\mathrm{e}}^{\sharp}) \quad \text{with} \quad \hat{\mathbf{N}}_{\mathrm{d}}^{\natural} = \partial_{[\hat{\mathbf{M}}_{\mathrm{d}}^{\natural}]^{\mathrm{t}}}{}^{\mathrm{pla}}\Phi^{\mathrm{p}}
\end{aligned} \tag{51}$$

which has a surprisingly similar structure compared to Equation (37).

Remark 5.1
For the sake of transparency, consider the isotropic case of a spherical damage mapping with $\|\bar{\mathbf{F}}^{\natural}\| \doteq \sqrt{3[1-D]}$. The proposed framework then boils down to the classical isotropic $[1-D]$ damage formulation with coupling to plasticity, see e.g. References [30, 31].

5.3.1. Prototype model. Concerning the plastic part of the dissipation function, the evolution of the damage spin is neglected for clarity's sake and thus the rotational term of $\bar{\mathbf{f}}^{\natural}$ is not incorporated; for a discussion on plastic spin, we refer to Reference [32] and references cited therein. In this context, the polar decomposition theorem yields

$$\begin{aligned}
\bar{\mathbf{F}}^{\natural} &= \bar{\mathbf{R}}^{\natural} \cdot \bar{\mathbf{U}}^{\natural} = \hat{\mathbf{V}}^{\natural} \cdot \bar{\mathbf{R}}^{\natural}, & \bar{\mathbf{f}}^{\natural} &= \bar{\mathbf{r}}^{\natural} \cdot \hat{\mathbf{u}}^{\natural} = \bar{\mathbf{v}}^{\natural} \cdot \bar{\mathbf{r}}^{\natural} \\
\bar{\mathbf{R}}^{\natural} &: T\bar{\mathscr{B}} \to T\mathscr{B}_{\mathrm{p}}, & \bar{\mathbf{r}}^{\natural} &: T\mathscr{B}_{\mathrm{p}} \to T\bar{\mathscr{B}} \\
\bar{\mathbf{U}}^{\natural} &: T^*\bar{\mathscr{B}} \times T\bar{\mathscr{B}} \to \mathbb{R}, & \hat{\mathbf{u}}^{\natural} &: T^*\mathscr{B}_{\mathrm{p}} \times T\mathscr{B}_{\mathrm{p}} \to \mathbb{R} \\
\hat{\mathbf{V}}^{\natural} &: T^*\mathscr{B}_{\mathrm{p}} \times T\mathscr{B}_{\mathrm{p}} \to \mathbb{R}, & \bar{\mathbf{v}}^{\natural} &: T^*\bar{\mathscr{B}} \times T\bar{\mathscr{B}} \to \mathbb{R}
\end{aligned} \tag{52}$$

with $[\bar{\mathbf{R}}^{\natural}]^{\mathrm{t}}=[\bar{\mathbf{R}}^{\natural}]^{-1}=\bar{\mathbf{r}}^{\natural}$ and $\det\bar{\mathbf{R}}^{\natural}=1$ whereby $\hat{\mathbf{u}}^{\natural}$, $\hat{\mathbf{V}}^{\natural}$ and $\bar{\mathbf{v}}^{\natural}$, $\bar{\mathbf{U}}^{\natural}$ turn out to be symmetric with respect to $\hat{\mathbf{G}}^{\natural}$ and $\bar{\mathbf{G}}^{\natural}$, respectively. Furthermore, note that the fictitious right and left stretch tensors are now determined by the damage metric tensor $\hat{\mathbf{A}}^{\sharp}$ if the rotational part equals the identity mapping; $\bar{\mathbf{R}}^{\natural}\equiv\bar{\mathbf{r}}^{\natural}$. In particular, we obtain

$$\hat{\mathbf{A}}^{\sharp}\equiv\bar{\mathbf{U}}^{\natural}\cdot\bar{\mathbf{G}}^{\sharp}\cdot[\bar{\mathbf{U}}^{\natural}]^{\mathrm{t}}\equiv\hat{\mathbf{V}}^{\natural}\cdot\bar{\mathbf{G}}^{\sharp}\cdot[\hat{\mathbf{V}}^{\natural}]^{\mathrm{t}},\quad[\hat{\mathbf{A}}^{\sharp}]^{-1}\equiv[\hat{\mathbf{u}}^{\natural}]^{\mathrm{t}}\cdot\bar{\mathbf{G}}^{\flat}\cdot\hat{\mathbf{u}}^{\natural}\equiv[\bar{\mathbf{v}}^{\natural}]^{\mathrm{t}}\cdot\bar{\mathbf{G}}^{\flat}\cdot\bar{\mathbf{v}}^{\natural}\tag{53}$$

With these assumptions at hand, the following restricted format of the plastic dissipation function is a natural outcome,

$$\begin{aligned}{}^{\mathrm{pla}}\Phi^{\mathrm{p}}&\doteq{}^{\mathrm{pla}}\Phi^{p}([[[\bar{\mathbf{v}}^{\natural}]^{\mathrm{t}}\bar{\otimes}[\bar{\mathbf{v}}^{\natural}]^{\mathrm{t}}]:\hat{\mathbf{C}}_{\mathrm{e}}^{\flat}]\cdot\hat{\mathbf{S}}^{\sharp};\hat{\mathbf{G}}^{\natural})\\&={}^{\mathrm{pla}}\Phi^{\mathrm{p}}([\hat{\mathbf{M}}^{\natural}_{\mathrm{d}\,[\bar{v}^{\natural}]^{\mathrm{t}}}]^{\mathrm{t}};\hat{\mathbf{G}}^{\natural})={}^{\mathrm{pla}}\Phi^{\mathrm{p}}({}^{\hat{G}^{\natural}[\hat{M}^{\natural}_{\mathrm{d}\,[\bar{v}^{\natural}]^{\mathrm{t}}}]^{\mathrm{t}}}I_{1,2,3})\end{aligned}\tag{54}$$

whereby a similar abbreviation as defined in Equation (49) has been applied. Recall that the alternative representation of the invariants, which was directly related to the postulate of effective stress referring to the fictitious configuration, results in the representation ${}^{\mathrm{pla}}\Phi^{\mathrm{p}}(\hat{\mathbf{C}}_{\mathrm{e}}^{\flat}\cdot[[\hat{\mathbf{u}}^{\natural}\bar{\otimes}\hat{\mathbf{u}}^{\natural}]:\hat{\mathbf{S}}^{\sharp}];\hat{\mathbf{G}}^{\natural})$. Next, we define a stress deviator with respect to the intermediate configuration (recall $\tilde{\mathbf{p}}^{\sharp}\doteq\tilde{\mathbf{g}}^{\sharp}$)

$$\begin{aligned}{}^{\mathrm{dev}}\tilde{\boldsymbol{\tau}}^{\sharp}&\doteq\tilde{\boldsymbol{\tau}}^{\sharp}-\tfrac{1}{3}[\tilde{\mathbf{p}}^{\flat}:\tilde{\boldsymbol{\tau}}^{\sharp}]\tilde{\mathbf{p}}^{\sharp}\\{}^{\mathrm{dev}}\hat{\mathbf{S}}^{\sharp}&\doteq\hat{\mathbf{S}}^{\sharp}-\tfrac{1}{3}[\hat{\mathbf{C}}^{\flat}_{\mathrm{e}[\bar{v}^{\natural}]^{\mathrm{t}}}:\hat{\mathbf{S}}^{\sharp}]\hat{\mathbf{B}}^{\sharp}_{\mathrm{e}\bar{U}^{\natural}}\\{}^{\mathrm{dev}}[\hat{\mathbf{M}}^{\natural}_{\mathrm{d}[\bar{v}^{\natural}]^{\mathrm{t}}}]^{\mathrm{t}}&\doteq[\hat{\mathbf{M}}^{\natural}_{\mathrm{d}[\bar{v}^{\natural}]^{\mathrm{t}}}]^{\mathrm{t}}-\tfrac{1}{3}[\hat{\mathbf{G}}^{\natural}:[\hat{\mathbf{M}}^{\natural}_{\mathrm{d}[\bar{v}^{\natural}]^{\mathrm{t}}}]^{\mathrm{t}}][\hat{\mathbf{G}}^{\natural}]^{\mathrm{t}}=\hat{\mathbf{C}}^{\flat}_{\mathrm{e}[\bar{v}^{\natural}]^{\mathrm{t}}}\cdot{}^{\mathrm{dev}}\hat{\mathbf{S}}^{\sharp}\end{aligned}\tag{55}$$

which allows the setup of a v. Mises-type function

$${}^{\mathrm{pla}}\Phi^{\mathrm{p}}([\hat{\mathbf{M}}_{\mathrm{d}[\bar{v}^{\natural}]^{\mathrm{t}}}]^{\mathrm{t}};\hat{\mathbf{G}}^{\natural})\doteq{}^{\hat{G}^{\natural}\,{}^{\mathrm{dev}}[\hat{M}^{\natural}_{\mathrm{d}\,[\bar{v}^{\natural}]^{\mathrm{t}}}]^{\mathrm{t}}}I_2=\hat{\mathbf{G}}^{\natural}:[\hat{\mathbf{C}}^{\flat}_{\mathrm{e}[\bar{v}^{\natural}]^{\mathrm{t}}}\cdot{}^{\mathrm{dev}}\hat{\mathbf{S}}^{\sharp}]^2\tag{56}$$

Finally, for completeness, we take the relation

$${}^{\mathrm{dev}^{\natural}}\hat{\mathbf{G}}^{\natural}\doteq\partial_{[\hat{\mathbf{M}}^{\natural}_{\mathrm{d}[\bar{v}^{\natural}]^{\mathrm{t}}}]^{\mathrm{t}}}{}^{\mathrm{dev}}[\hat{\mathbf{M}}^{\natural}_{\mathrm{d}[\bar{v}^{\natural}]^{\mathrm{t}}}]^{\mathrm{t}}=[\hat{\mathbf{G}}^{\natural}]^{\mathrm{t}}\bar{\otimes}\hat{\mathbf{G}}^{\natural}-\tfrac{1}{3}[\hat{\mathbf{G}}^{\natural}]^{\mathrm{t}}\otimes\hat{\mathbf{G}}^{\natural}\tag{57}$$

into account, ${}^{\mathrm{dev}^{\natural}}\hat{\mathbf{G}}^{\natural}:[\hat{\mathbf{M}}^{\natural}_{\mathrm{d}[\bar{v}^{\natural}]^{\mathrm{t}}}]^{\mathrm{t}}={}^{\mathrm{dev}}[\hat{\mathbf{M}}^{\natural}_{\mathrm{d}[\bar{v}^{\natural}]^{\mathrm{t}}}]^{\mathrm{t}}$ being obvious, and with these definitions at hand the v. Mises-type model results in the associated evolution equation

$$\begin{aligned}\hat{\mathbf{L}}^{\natural}_{\mathrm{p}}&=\mathrm{D}_t\lambda\hat{\mathbf{N}}^{\natural}_{[\bar{v}^{\natural}]^{\mathrm{t}}}(\hat{\mathbf{N}}^{\natural}_{\mathrm{d}},\hat{\mathbf{C}}^{\flat}_{\mathrm{e}[\bar{v}^{\natural}]^{\mathrm{t}}},\hat{\mathbf{B}}^{\sharp}_{\mathrm{e}})\\\text{with}\quad\hat{\mathbf{N}}^{\natural}_{\mathrm{d}}&=\partial_{{}^{\mathrm{dev}}[\hat{\mathbf{M}}^{\natural}_{\mathrm{d}[\bar{v}^{\natural}]^{\mathrm{t}}}]^{\mathrm{t}}}{}^{\mathrm{pla}}\Phi^{\mathrm{p}}:{}^{\mathrm{dev}^{\natural}}\hat{\mathbf{G}}^{\natural}=2\,{}^{\mathrm{dev}}[\hat{\mathbf{M}}^{\natural}_{\mathrm{d}[\bar{v}^{\natural}]^{\mathrm{t}}}]^{\mathrm{t}}:[[\hat{\mathbf{G}}^{\natural}]^{\mathrm{t}}\underline{\otimes}\hat{\mathbf{G}}^{\natural}]\\\text{and}\quad\hat{\mathbf{C}}^{\flat}_{\mathrm{e}[\bar{v}^{\natural}]^{\mathrm{t}}}&=[[\bar{\mathbf{v}}^{\natural}]^{\mathrm{t}}\bar{\otimes}[\bar{\mathbf{v}}^{\natural}]^{\mathrm{t}}]:[[\mathbf{F}^{\natural}_{\mathrm{e}}]^{\mathrm{t}}\cdot\mathbf{g}^{\flat}\cdot\mathbf{F}^{\natural}_{\mathrm{e}}]\\\text{for}\quad[\hat{\mathbf{A}}^{\sharp}]^{-1}&\equiv[\bar{\mathbf{v}}^{\natural}]^{\mathrm{t}}\cdot\bar{\mathbf{G}}^{\flat}\cdot\bar{\mathbf{v}}^{\natural}\\\text{and}\quad\hat{\mathbf{B}}^{\sharp}_{\mathrm{e}}&=\mathbf{f}^{\natural}_{\mathrm{e}}\cdot\mathbf{g}^{\sharp}\cdot[\mathbf{f}^{\natural}_{\mathrm{e}}]^{\mathrm{t}}\end{aligned}\tag{58}$$

compare Equation (51).

6. INTEGRATION OF THE EVOLUTION EQUATIONS

Let the time interval of interest be given by N time steps $\mathbb{T} = \bigcup_{n=0}^{N} [{}^{n}t, {}^{n+1}t]$. In the following we highlight a strain driven staggered algorithm with respect to the Lagrange multiplier $\mathrm{D}_t\lambda$ and the variables $\mathbf{F}_{\mathrm{e}}^{\natural}$, $\hat{\mathbf{A}}^{\sharp}$, κ. Recall that loading and unloading have to be checked by each trial step at ${}^{n+1}\mathbf{F}^{\natural}$. Thereby, in view of the iteration for the Lagrange multiplier, usual scalar-valued schemes can be applied, e.g. Newton's method or regula-falsi-type algorithms. For an outline of the numerical setting for multiplicative elasto-plasticity, we refer to References [26, 33].

Owing to the non-coaxiality of the damage metric tensor and the correlated flow direction—for the general anisotropic framework—no exponential integration scheme as in the isotropic case is conveniently available. Thus the simplest implicit integration technique, i.e. Euler backward, is applied for both damage types throughout this contribution. In this context, we obtain for the quasi isotropic setting

$$ {}^{n+1}\hat{\mathbf{A}}^{\sharp} = {}^{n}\hat{\mathbf{A}}^{\sharp} + \Delta\lambda\delta_1 [\, {}^{n+1}\hat{\mathbf{Z}}^{\flat} : {}^{n+1}\hat{\mathbf{A}}^{\sharp}] \, {}^{n+1}\hat{\mathbf{A}}^{\sharp} \tag{59} $$

and concerning the general anisotropic case, one ends up with

$$ {}^{n+1}\hat{\mathbf{A}}^{\sharp} = {}^{n}\hat{\mathbf{A}}^{\sharp} + \Delta\lambda\delta_2 \, {}^{n+1}\hat{\mathbf{A}}^{\sharp} \cdot {}^{n+1}\hat{\mathbf{Z}}^{\flat} \cdot {}^{n+1}\hat{\mathbf{A}}^{\sharp} \tag{60} $$

The application of different higher order Runge–Kutta integration schemes in the present context is discussed in Reference [29].

For the hardening variable, we once more adopt an Euler backward integration which results in

$$ {}^{n+1}\kappa = {}^{n}\kappa + \Delta\lambda \, \tfrac{2}{3}[Y_0 - H] \tag{61} $$

Although plastic incompressibility is not a key issue here since plasticity is coupled to continuum damage, we apply an exponential integration scheme for $\mathbf{F}_{\mathrm{p}}^{\natural}$. The corresponding evolution equation is constructed via Equations (28) and (58) and reads as

$$ \mathrm{D}_t\mathbf{F}_{\mathrm{p}}^{\natural} \cdot \mathbf{f}_{\mathrm{p}}^{\natural} = \hat{\mathbf{L}}_{\mathrm{p}}^{\natural} = \mathrm{D}_t\lambda \hat{\mathbf{N}}_{[\bar{f}^{\natural}]^{\mathrm{t}}}^{\natural} \;\Rightarrow\; \mathrm{D}_t\mathbf{F}_{\mathrm{p}}^{\natural} = \mathrm{D}_t\lambda \hat{\mathbf{N}}_{[\bar{f}^{\natural}]^{\mathrm{t}}}^{\natural} \cdot \mathbf{F}_{\mathrm{p}}^{\natural} \tag{62} $$

Based on this, straightforward application of the exponential integration scheme results in

$$ {}^{n+1}\mathbf{F}_{\mathrm{p}}^{\natural} = \exp(\Delta\lambda \, {}^{n+1}\hat{\mathbf{N}}_{[\bar{f}^{\natural}]^{\mathrm{t}}}^{\natural}) \cdot {}^{n}\mathbf{F}_{\mathrm{p}}^{\natural} \;\Rightarrow\; {}^{n+1}\mathbf{f}_{\mathrm{p}}^{\natural} = {}^{n}\mathbf{f}_{\mathrm{p}}^{\natural} \cdot \exp(-\Delta\lambda \, {}^{n+1}\hat{\mathbf{N}}_{[\bar{f}^{\natural}]^{\mathrm{t}}}^{\natural}) \tag{63} $$

see Reference [34]. In this direction, the elastic part of the deformation gradient allows the representation

$$ {}^{n+1}\mathbf{F}_{\mathrm{e}}^{\natural} = {}^{n+1}\mathbf{F}^{\natural} \cdot {}^{n+1}\mathbf{f}_{\mathrm{p}}^{\natural} = {}^{n+1}\mathbf{F}_{\mathrm{etri}}^{\natural} \cdot \exp(-\Delta\lambda \, {}^{n+1}\hat{\mathbf{N}}_{[\bar{f}^{\natural}]^{\mathrm{t}}}^{\natural}) \tag{64} $$

whereby ${}^{n+1}\hat{\mathbf{N}}_{[\bar{f}^{\natural}]^{\mathrm{t}}}^{\natural}$ is obviously not coaxial to ${}^{n+1}\hat{\mathbf{C}}_{\mathrm{e}}^{\flat} = [\, {}^{n+1}\mathbf{F}_{\mathrm{e}}^{\natural}]^{\mathrm{t}} \cdot \mathbf{g}^{\flat} \cdot {}^{n+1}\mathbf{F}_{\mathrm{e}}^{\natural}$, compare Equations (52) and (58).

With these integration schemes at hand, we are able to set up an outline of the applied algorithm which reads for the above mentioned staggered approach as follows:

(Finite Element Method) **for** given ${}^{n+1}\mathbf{F}^{\natural}$ **do**
if ${}^{\mathrm{yie}}\Phi^{\mathrm{p}}|_{n+1} > 0$ **then**
(scalar-valued iteration) **dowhile** $|\,{}^{\mathrm{yie}}\Phi^{\mathrm{p}}(\Delta\lambda)|_{n+1} > \mathrm{tol}$
$\Delta\lambda = \cdots$
(Newton-type method) **dowhile** $\|{}^{\mathrm{dam}}\hat{\mathbf{R}}^{\flat}\| + \|\,{}^{\mathrm{pla}}\mathbf{R}^{\natural}\| + |\,{}^{\mathrm{har}}R| > \mathrm{tol}$
$\cdots$

$$
\begin{aligned}
{}^{n+1}\hat{\mathbf{A}}^{\sharp}_{k+1} &= {}^{n+1}\hat{\mathbf{A}}^{\sharp}_{k} + \Delta\hat{\mathbf{A}}^{\sharp} \\
{}^{n+1}\mathbf{F}^{\natural}_{\mathrm{e}k+1} &= {}^{n+1}\mathbf{F}^{\natural}_{\mathrm{e}k} + \Delta\mathbf{F}^{\natural}_{\mathrm{e}} \\
{}^{n+1}\kappa_{k+1} &= {}^{n+1}\kappa_{k} + \Delta\kappa
\end{aligned}
$$

enddo
enddo
endif

Here, we choose a modified regula falsi scheme for the iteration of the Lagrange multiplier and a Newton algorithm to compute the set of internal variables. This strategy results in the following system of linear equation within each Newton iteration

$$
\begin{bmatrix}
{}^{\mathrm{dam}}\hat{\mathbf{J}}^{\natural}_{\hat{\mathbf{A}}^{\sharp}} & {}^{\mathrm{dam}}\hat{\mathbf{J}}^{\natural}_{\mathbf{F}^{\natural}_{\mathrm{e}}} & \\
{}^{\mathrm{pla}}\mathbf{J}^{\natural}_{\hat{\mathbf{A}}^{\sharp}} & {}^{\mathrm{pla}}\mathbf{J}^{\natural}_{\mathbf{F}^{\natural}_{\mathrm{e}}} & \\
 & & {}^{\mathrm{har}}J_{\kappa}
\end{bmatrix}
\circ
\begin{bmatrix}
\Delta\hat{\mathbf{A}}^{\sharp} \\ \Delta\mathbf{F}^{\natural}_{\mathrm{e}} \\ \Delta\kappa
\end{bmatrix}
=
\begin{bmatrix}
-\,{}^{\mathrm{dam}}\hat{\mathbf{R}}^{\sharp} \\ -\,{}^{\mathrm{pla}}\mathbf{R}^{\natural} \\ -\,{}^{\mathrm{har}}R
\end{bmatrix}
\tag{65}
$$

whereby the notation $\circ$ denotes the appropriate type of contraction and additional abbreviations have been introduced, in particular the residua

$$
\begin{aligned}
{}^{\mathrm{dam}}\hat{\mathbf{R}}^{\sharp} &= {}^{n+1}\hat{\mathbf{A}}^{\sharp}_{k} - {}^{n}\hat{\mathbf{A}}^{\sharp} - \Delta\lambda\delta_2\,{}^{n+1}\hat{\mathbf{A}}^{\sharp}_{k}\cdot\,{}^{n+1}\hat{\Delta}^{\sharp}_{k}\cdot\,{}^{n+1}\hat{\mathbf{A}}^{\sharp}_{k} \\
{}^{\mathrm{pla}}\mathbf{R}^{\natural} &= {}^{n+1}\mathbf{F}^{\natural}_{\mathrm{e}\,k} - {}^{n+1}\mathbf{F}^{\natural}_{\mathrm{etri}}\cdot\exp(-\Delta\lambda\,{}^{n+1}\hat{\mathbf{N}}^{\natural}_{[f^{\natural}]^{\natural}k}) \\
{}^{\mathrm{har}}R &= {}^{n+1}\kappa_{k} - {}^{n}\kappa - \Delta\lambda\,\tfrac{2}{3}[Y_0 - {}^{n+1}H_{k}]
\end{aligned}
\tag{66}
$$

and the Jacobians

$$
\begin{aligned}
{}^{\mathrm{dam}}\hat{\mathbf{J}}^{\natural}_{\hat{\mathbf{A}}^{\sharp}} &= \partial_{{}^{n+1}\hat{\mathbf{A}}^{\sharp}_{k}}\,{}^{\mathrm{dam}}\hat{\mathbf{R}}^{\sharp}, \quad {}^{\mathrm{dam}}\hat{\mathbf{J}}^{\natural}_{\mathbf{F}^{\natural}_{\mathrm{e}}} = \partial_{{}^{n+1}\mathbf{F}^{\natural}_{\mathrm{e}\,k}}\,{}^{\mathrm{dam}}\hat{\mathbf{R}}^{\sharp} \\
{}^{\mathrm{pla}}\mathbf{J}^{\natural}_{\hat{\mathbf{A}}^{\sharp}} &= \partial_{{}^{n+1}\hat{\mathbf{A}}^{\sharp}_{k}}\,{}^{\mathrm{pla}}\mathbf{R}^{\natural}, \quad {}^{\mathrm{pla}}\mathbf{J}^{\natural}_{\mathbf{F}^{\natural}_{\mathrm{e}}} = \partial_{{}^{n+1}\mathbf{F}^{\natural}_{\mathrm{e}\,k}}\,{}^{\mathrm{pla}}\mathbf{R}^{\natural} \\
{}^{\mathrm{har}}J_{\kappa} &= \partial_{{}^{n+1}\kappa_{k}}\,{}^{\mathrm{har}}R
\end{aligned}
\tag{67}
$$

An outline on the 'exact' derivation of a Jacobian similar to ${}^{\mathrm{pla}}\mathbf{J}^{\natural}_{\mathbf{F}^{\natural}_{\mathrm{e}}}$ is discussed by de Souza Neto [35]. We nevertheless adopt a numerical perturbation scheme in this contribution to compute the Jacobians for the subsequent numerical examples. Moreover, within a finite element setting, it turns out to be advantageous to apply this finite difference approximation in addition to the global tangent operator. For convenience of the reader, Appendix A reiterates the adopted algorithm.

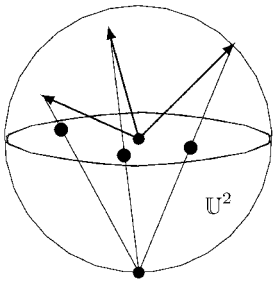

Figure 2. Stereographic projection.

7. EXAMPLES

Within the following numerical examples, where we discuss the overall anisotropic behaviour of the proposed framework, a typical compressible Neo–Hook material is adopted. In particular we choose

$$\begin{aligned} {}^{\mathrm{dam}}\psi_0^{\mathrm{p}} &= \frac{\mu}{2}[\,{}^{\hat{C}_{\mathrm{e}}^{\flat}\hat{A}^{\sharp}}J_1 - 3] - \mu \ln({}^{\hat{C}_{\mathrm{e}}^{\flat}\hat{A}^{\sharp}}J_3) + \frac{\lambda}{2}\ln^2({}^{\hat{C}_{\mathrm{e}}^{\flat}\hat{A}^{\sharp}}J_3) \quad \text{with} \\ {}^{\hat{C}_{\mathrm{e}}^{\flat}\hat{A}^{\sharp}}J_1 &= 3 + 2\,{}^{\hat{E}_{\mathrm{e}}^{\flat}\hat{A}^{\sharp}}I_1 \\ {}^{\hat{C}_{\mathrm{e}}^{\flat}\hat{A}^{\sharp}}J_3 &= 1 + 2\,{}^{\hat{E}_{\mathrm{e}}^{\flat}\hat{A}^{\sharp}}I_1 - 2\,{}^{\hat{E}_{\mathrm{e}}^{\flat}\hat{A}^{\sharp}}I_2 + \tfrac{8}{3}\,{}^{\hat{E}_{\mathrm{e}}^{\flat}\hat{A}^{\sharp}}I_3 + 2\,{}^{\hat{E}_{\mathrm{e}}^{\flat}\hat{A}^{\sharp}}I_1^2 - 4\,{}^{\hat{E}_{\mathrm{e}}^{\flat}\hat{A}^{\sharp}}I_1\,{}^{\hat{E}_{\mathrm{e}}^{\flat}\hat{A}^{\sharp}}I_2 + \tfrac{4}{3}\,{}^{\hat{E}_{\mathrm{e}}^{\flat}\hat{A}^{\sharp}}I_1^3 \end{aligned} \tag{68}$$

Moreover, concerning the hardening part of the free Helmholtz energy function, we account for the established additive decomposition into a saturation-type contribution and a quadratic term with respect to the scalar-valued hardening variable

$${}^{\mathrm{har}}\psi_0(\kappa) \doteq [Y_\infty - Y_0][\kappa + \delta_3^{-1}\exp(-\delta_3\kappa) - \delta_3^{-1}] + \tfrac{1}{2}\,\delta_4\kappa^2 \tag{69}$$

with $Y_\infty, Y_0, \delta_{3,4} \in \mathbb{R}_+$ and $Y_\infty \geqslant Y_0$. The hardening stress consequently results in

$$H(\kappa) = [Y_0 - Y_\infty][1 - \exp(-\delta_3\kappa)] - \delta_4\kappa \tag{70}$$

In order to highlight the principal directions of specific symmetric second order tensors, like e.g. stress and strain, the method of stereographic projection is applied which is well-known from crystallography and represents a homomorphism $\mathbb{O}_+^3 \to \mathbb{M}^2$, see Figure 2 for an illustration. Moreover, in case that two tensors—say $\hat{\mathbf{E}}_{\mathrm{e}}^{\flat}$ and $\hat{\mathbf{S}}^{\sharp}$—are not coaxial, we can compute a non-vanishing scalar

$$\delta(\hat{\mathbf{E}}_{\mathrm{e}}^{\flat}, \hat{\mathbf{S}}^{\sharp}) = \frac{\|\hat{\mathbf{G}}^{\flat}\cdot\hat{\mathbf{S}}^{\sharp}\cdot\hat{\mathbf{E}}_{\mathrm{e}}^{\flat} - \hat{\mathbf{E}}_{\mathrm{e}}^{\flat}\cdot\hat{\mathbf{S}}^{\sharp}\cdot\hat{\mathbf{G}}^{\flat}\|}{\|\hat{\mathbf{S}}^{\sharp}\|\|\hat{\mathbf{E}}_{\mathrm{e}}^{\flat}\|} \tag{71}$$

which we call anisotropy measure. In addition, the preferred direction of the initial anisotropy metric or rather damage metric tensor can be determined by spherical co-ordinates, say $\vartheta^{1,2}$. Assuming a Cartesian frame, one possible representation of ${}^{A}\mathbf{N}_\zeta = \sum_{i=1}^{3}\,{}^{A}N_\zeta^i\,\mathbf{e}_i \in \mathbb{U}^2$ reads as

$${}^{A}N_\zeta^1 = \sin(\vartheta_\zeta^1)\,\sin(\vartheta_\zeta^2), \quad {}^{A}N_\zeta^2 = \cos(\vartheta_\zeta^2), \quad {}^{A}N_\zeta^3 = \cos(\vartheta_\zeta^1)\,\sin(\vartheta_\zeta^2) \tag{72}$$

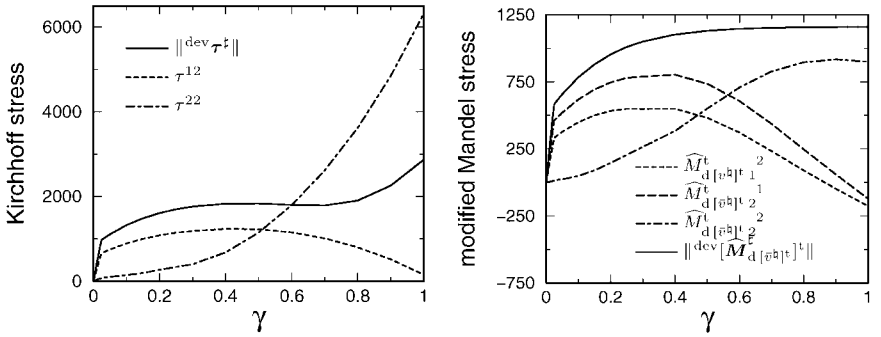

Figure 3. Simple shear, anisotropic elasto-plasticity: Kirchhoff stress $\boldsymbol{\tau}^{\sharp}$ and modified Mandel stress $[\hat{\mathbf{M}}^{\sharp}_{\mathrm{d}\,[\bar{v}^{\sharp}]^{t}}]^{t}$.

7.1. Homogeneous deformation in simple shear

For the discussion of a homogeneous deformation in simple shear ($\mathbf{F}=\mathbf{I}+\gamma\,\mathbf{e}_1\otimes\mathbf{e}_2$ with respect to a Cartesian frame $\mathbf{e}_i$ and $\mathbf{I}=\delta_{ij}\,\mathbf{e}_i\otimes\mathbf{e}_j$), the setting of anisotropic elasto-plasticity and the coupling to quasi isotropic and anisotropic damage are considered. In both cases the initial anisotropy, or rather damage metric $\hat{\mathbf{A}}^{\sharp}|_{t_0}$ is assumed to be non-spherical. In particular, we choose the anisotropy metric to be determined by the spherical co-ordinates $\vartheta_1^1=\frac{5}{6}\,\pi,\ \vartheta_1^2=\frac{1}{6}\,\pi,\ \vartheta_2^1=\frac{1}{3}\,\pi,\ \vartheta_2^2=\frac{1}{2}\,\pi$ and the scalars $\alpha_0=1,\ \alpha_1=1/4,\ \alpha_2=1/2$, see Equations (21) and (72). Thus, from the beginning, the elastic behaviour is anisotropic. The material parameters for the Neo–Hook material, Equation (68), are assumed as $\mu=10^4,\ \lambda=10^3$. Moreover, let the hardening part be determined by $Y_0=10^3,\ \ Y_\infty=2\times10^3$ and $\delta_{3,4}=10$.

It is clearly seen in the subsequent numerical examples that the evolution of the deviatoric norm of the modified Mandel tensor $\|^{\mathrm{dev}}[\hat{\mathbf{M}}^{\sharp}_{\mathrm{d}\,[\bar{v}^{\sharp}]^{t}}]^{t}\|$, which essentially enters the yield function, displays a typical saturation effect. Contrary, due to the incorporated continuum damage, the corresponding norm of the spatial Kirchhoff stress $\|^{\mathrm{dev}}\boldsymbol{\tau}^{\sharp}\|$, decreases. In the sequel, components of tensorial fields refer to Cartesian frames, e.g. $[\bullet]^{ij}=\mathbf{e}^i\cdot[\bullet]^{\sharp}\cdot\mathbf{e}^j$.

7.1.1. Anisotropic elasto-plasticity. To set the stage, we firstly discuss a purely elasto-plastic body whereby no damage evolution takes place, $\delta_{1,2}=0$. In this context, Figures 3–5 highlight the overall anisotropic behaviour. Representative properties of the Kirchhoff stress and the non-symmetric, modified Mandel tensor are given in Figure 3. The anisotropy measure in terms of strain and stress, $\delta(\hat{\mathbf{E}}^{\flat}_{\mathrm{e}},\hat{\mathbf{S}}^{\sharp})$, shows a strong dependence on the shear number γ and, due to the fact that no damage evolution is incorporated, all eigenvalues of the anisotropy metric remain constant during the deformation process, see Figure 4. In addition, the non-coaxiality of stress and strain is highlighted in Figures 5 for different shear numbers γ by applying the method of stereographic projection. Next, we reverse the shear direction and consider unloading/reloading with respect to the deformation history $\gamma\in[0\to1,1\to0]$. Figures 6 and 7 monitor the contributions of the Kirchhoff stress, the modified Mandel stress, the anisotropy measure and the damage eigenvalues which are trivially constant for the considered setting.

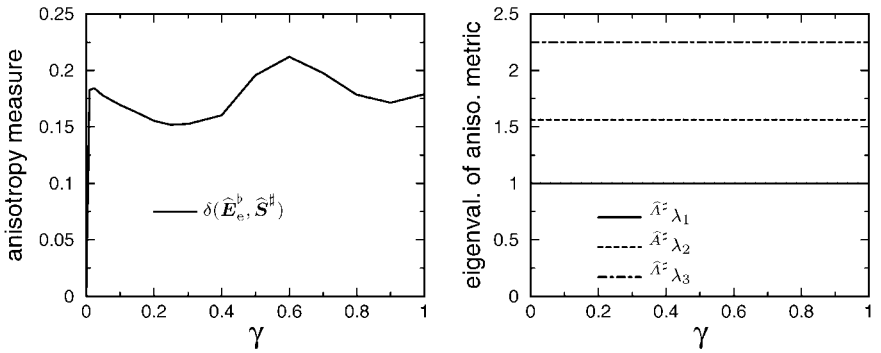

Figure 4. Simple shear, anisotropic elasto-plasticity: Anisotropy measure $\delta(\hat{\mathbf{E}}_e^\flat, \hat{\mathbf{S}}^\sharp)$ and eigenvalues of the anisotropy metric ${}^{\hat{A}^\sharp}\lambda_{1,2,3}$.

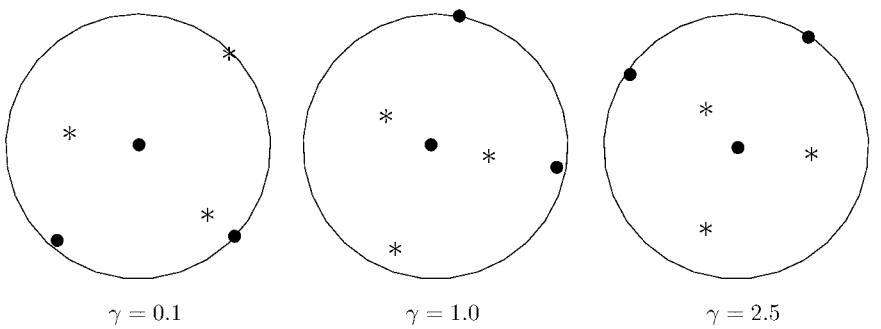

Figure 5. Simple shear, anisotropic elasto-plasticity: Stereographic projection of strain ($\hat{\mathbf{E}}_e^\flat : \bullet$) and stress ($\hat{\mathbf{S}}^\sharp : *$).

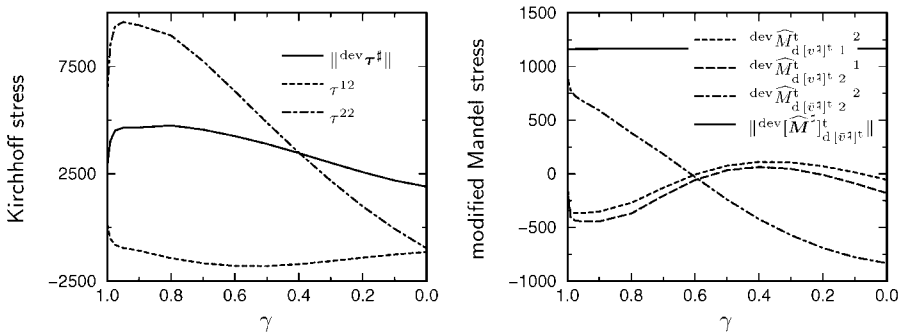

Figure 6. Simple shear, anisotropic elasto-plasticity: Kirchhoff stress $\boldsymbol{\tau}^\sharp$ and modified Mandel stress $[\hat{\mathbf{M}}^\natural_{\mathrm{d}[\bar{v}^\sharp]^{\mathrm{t}}}]^{\mathrm{t}}$.

Against intuition, we do not observe an exclusive reloading behaviour as experienced in an isotropic setting, i.e. $\hat{\mathbf{A}}^\sharp \propto \hat{\mathbf{G}}^\sharp$. Apparently, this immediate loading effect results from the incorporated anisotropy and the comparatively small threshold. Finally, in analogy to Figure 5

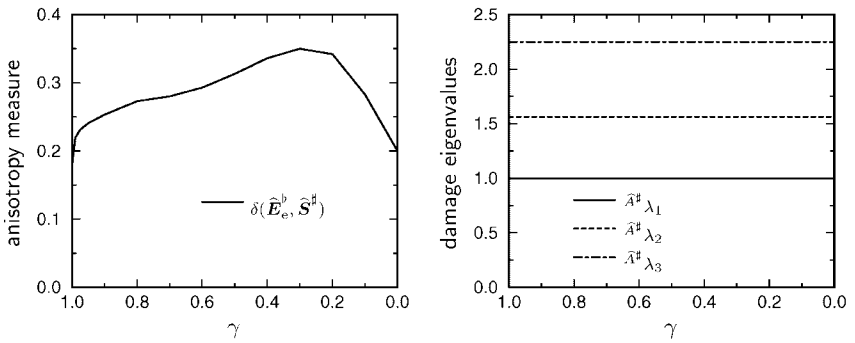

Figure 7. Simple shear, anisotropic elasto-plasticity: Anisotropy measure $\delta(\hat{\mathbf{E}}_e^{\flat}, \hat{\mathbf{S}}^{\sharp})$ and eigenvalues of the anisotropy metric ${}^{\hat{A}^{\sharp}}\lambda_{1,2,3}$.

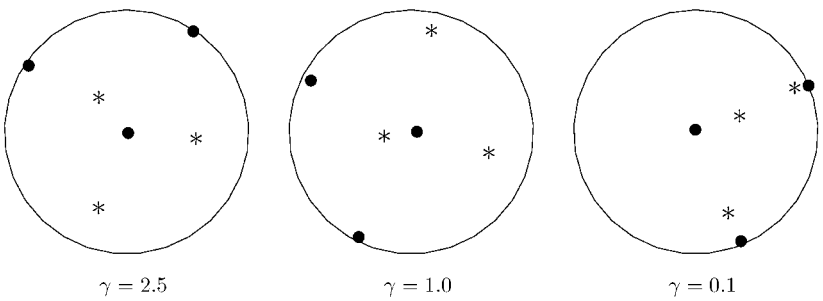

Figure 8. Simple shear, anisotropic elasto-plasticity: Stereographic projection of strain ($\hat{\mathbf{E}}_e^{\flat} : \bullet$) and stress ($\hat{\mathbf{S}}^{\sharp} : *$).

we discuss the evolution of the principal directions of strain and stress for reverse loading within the shear interval $\gamma \in [0 \to 2.5, 2.5 \to 0.1]$, see Figure 8.

7.1.2. Anisotropic elasto-plasticity coupled to quasi isotropic damage. Next, we consider the coupling to quasi isotropic damage, with $\delta_1 = 10^2$ and $\delta_2 = 0$. Similar to the previous setting, Figure 9 monitors the Kirchhoff stress and the non-symmetric, modified Mandel tensor. Now the eigenvalues of the damage metric decrease, see Figure 10. Apparently, these eigenvalues, ${}^{\hat{A}^{\sharp}}\lambda_{1,2,3}$, are uniformly scaled down during the deformation process which is due to the nature of quasi isotropic damage evolution. Moreover, Figure 11 highlights the non-commutativity of strain and stress for different shear numbers γ and the case of reverse loading is visualised in Figures 12–14 in analogy to Section 7.1.1.

7.1.3. Anisotropic elasto-plasticity coupled to anisotropic damage. Lastly, we take anisotropic damage evolution into account with $\delta_1 = 0$ and $\delta_2 = 10^2$. Figures 15–22 highlight the corresponding results in analogy to the previous settings. Please note that besides $\delta(\hat{\mathbf{E}}_e^{\flat}, \hat{\mathbf{S}}^{\sharp})$ Figures 16 and 20 monitor the anisotropy measure $\delta(\hat{\mathbf{A}}^{\sharp}, \hat{\mathbf{A}}^{\sharp}|_{t_0})$ which underlines the evolution

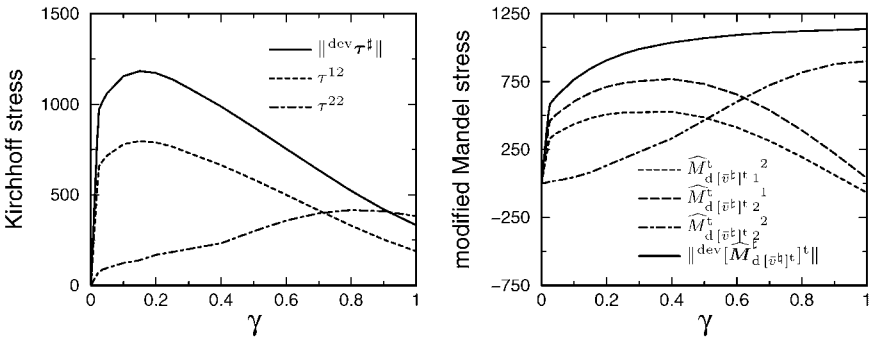

Figure 9. Simple shear, anisotropic elasto-plasticity coupled to quasi isotropic damage: Kirchhoff stress $\boldsymbol{\tau}^{\sharp}$ and modified Mandel stress $[\hat{\mathbf{M}}^{\sharp}_{\mathrm{d}\,[\bar{v}^{\sharp}]^{\mathrm{t}}}]^{\mathrm{t}}$.

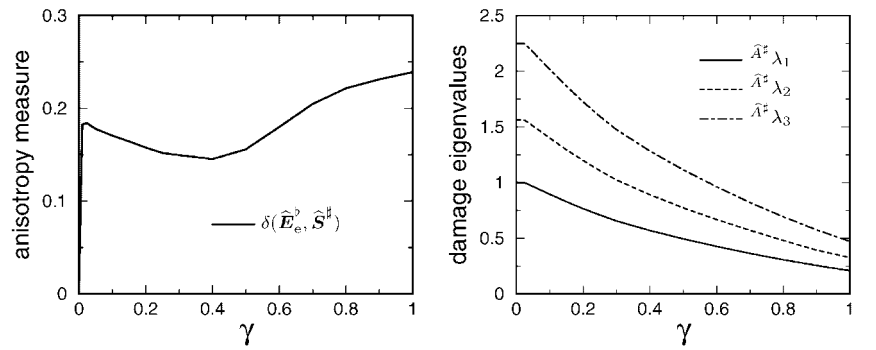

Figure 10. Simple shear, anisotropic elasto-plasticity coupled to quasi isotropic damage: Anisotropy measure $\delta(\hat{\mathbf{E}}^{\flat}_{\mathrm{e}}, \hat{\mathbf{S}}^{\sharp})$ and eigenvalues of the damage metric ${}^{\hat{A}^{\sharp}}\lambda_{1,2,3}$.

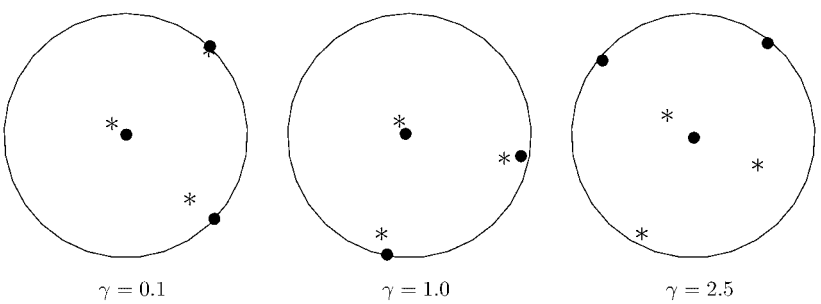

Figure 11. Simple shear, anisotropic elasto-plasticity coupled to quasi isotropic damage: Stereographic projection of strain ($\hat{\mathbf{E}}^{\flat}_{\mathrm{e}} : \bullet$) and stress ($\hat{\mathbf{S}}^{\sharp} : *$).

of the principal axes of the damage metric. Furthermore, due to the nature of anisotropic damage, the eigenvalues of the damage metric now degrade differently during the deformation process. The same effect is clearly reflected by the method of stereographic projection in

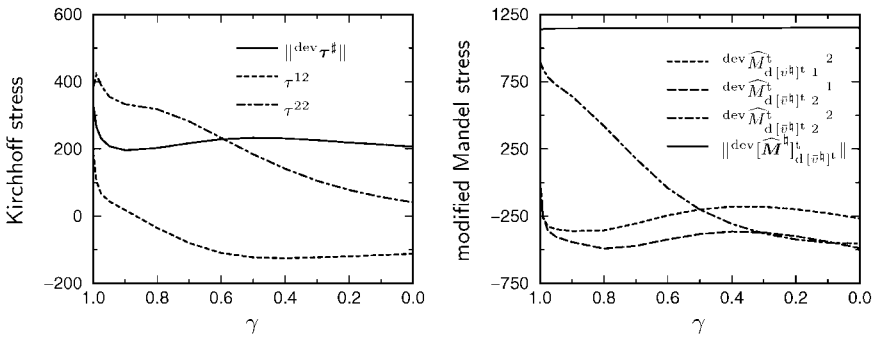

Figure 12. Simple shear, anisotropic elasto-plasticity coupled to quasi isotropic damage: Kirchhoff stress $\boldsymbol{\tau}^{\sharp}$ and modified Mandel stress $[\hat{\mathbf{M}}^{\sharp}_{\mathrm{d}\,[\bar{v}^{\sharp}]^{\mathrm{t}}}]^{\mathrm{t}}$.

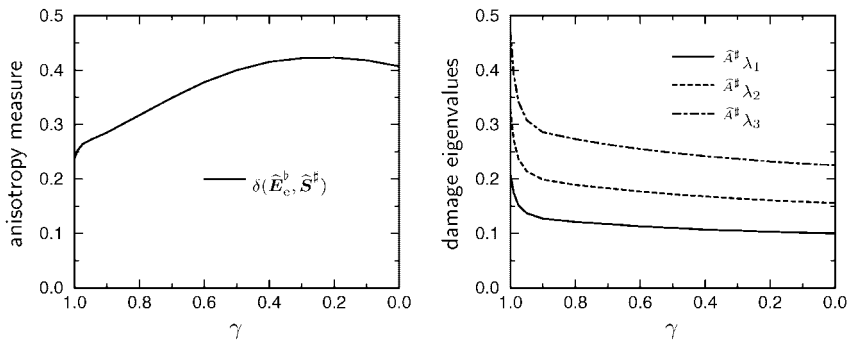

Figure 13. Simple shear, anisotropic elasto-plasticity coupled to quasi isotropic damage: Anisotropy measure $\delta(\hat{\mathbf{E}}^{\flat}_{\mathrm{e}}, \hat{\mathbf{S}}^{\sharp})$ and eigenvalues of the damage metric ${}^{\hat{A}^{\sharp}}\lambda_{1,2,3}$.

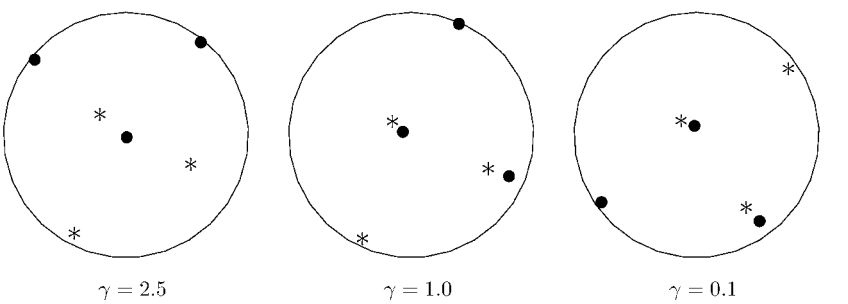

Figure 14. Simple shear, anisotropic elasto-plasticity coupled to quasi isotropic damage: Stereographic projection of strain ($\hat{\mathbf{E}}^{\flat}_{\mathrm{e}} : \bullet$) and stress ($\hat{\mathbf{S}}^{\sharp} : *$).

Figures 18 and 22 where the contributions of the actual damage metric $\hat{\mathbf{A}}^{\sharp}$ are compared to the initial damage metric $\hat{\mathbf{A}}^{\sharp}|_{t_0}$. Similar to the previous examples, Figures 17 and 21 visualize the non-coaxiality of strain and stress for different shear numbers γ.

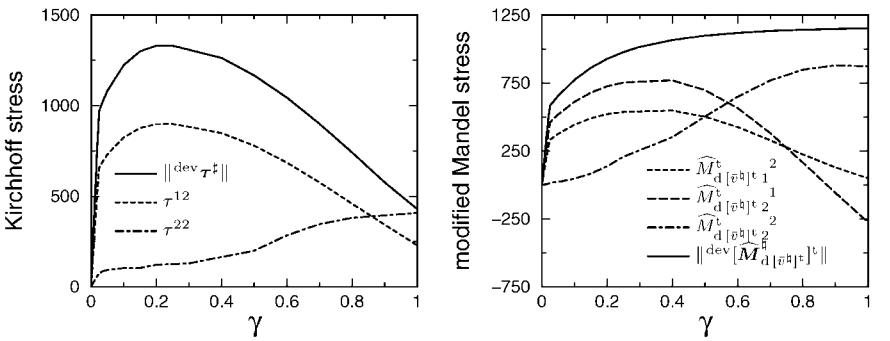

Figure 15. Simple shear, anisotropic elasto-plasticity coupled to anisotropic damage: Kirchhoff stress $\boldsymbol{\tau}^{\sharp}$ and modified Mandel stress $[\hat{\mathbf{M}}^{\sharp}_{\mathrm{d}\,[\bar{v}^{\sharp}]^{\mathrm{t}}}]^{\mathrm{t}}$.

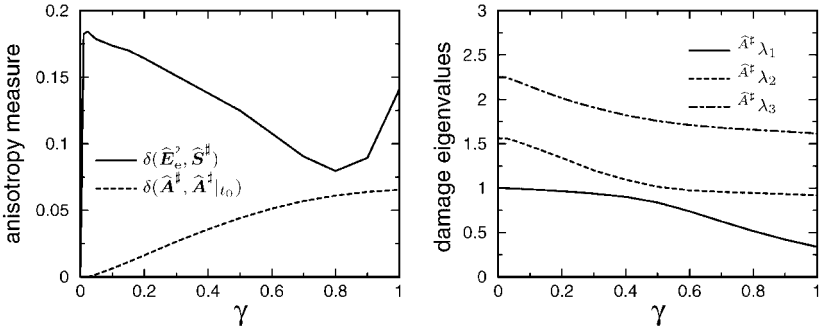

Figure 16. Simple shear, anisotropic elasto-plasticity coupled to anisotropic damage: Anisotropy measure $\delta(\hat{\mathbf{E}}^{\flat}_{\mathrm{e}}, \hat{\mathbf{S}}^{\sharp})$, $\delta(\hat{\mathbf{A}}^{\sharp}, \hat{\mathbf{A}}^{\sharp}|_{t_0})$ and eigenvalues of the damage metric ${}^{A^{\sharp}}\lambda_{1,2,3}$.

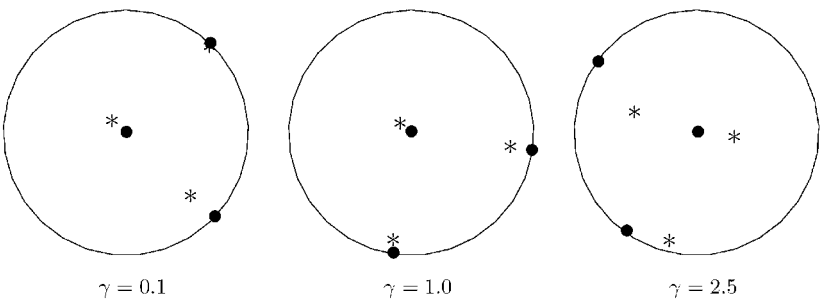

Figure 17. Simple shear, anisotropic elasto-plasticity coupled to anisotropic damage: Stereographic projection of strain ($\hat{\mathbf{E}}^{\flat}_{\mathrm{e}} : \bullet$) and stress ($\hat{\mathbf{S}}^{\sharp} : *$).

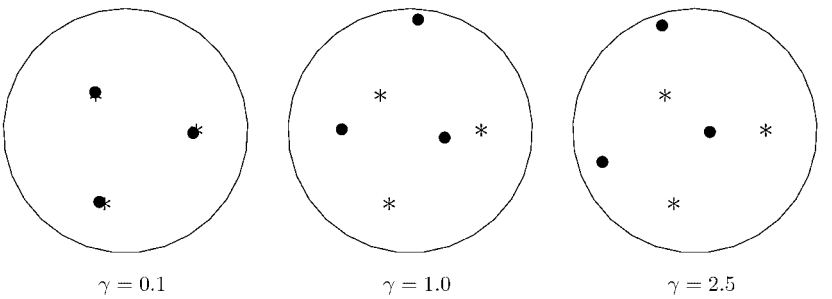

Figure 18. Simple shear, anisotropic elasto-plasticity coupled to anisotropic damage: Stereographic projection of the actual damage metric ($\hat{\mathbf{A}}^{\sharp} : \bullet$) and the initial damage metric ($\hat{\mathbf{A}}^{\sharp}|_{t_0} : *$).

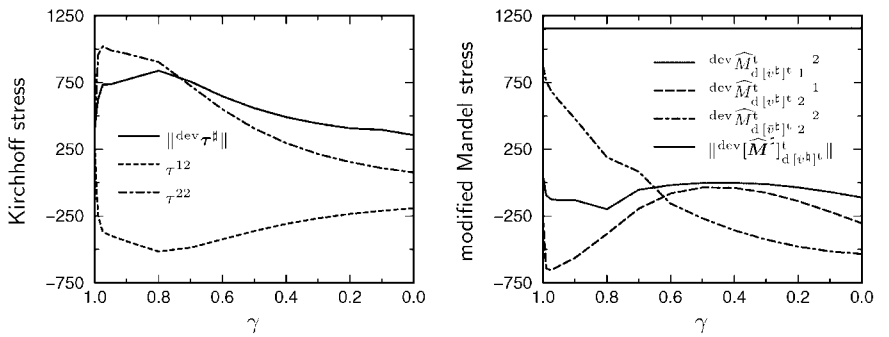

Figure 19. Simple shear, anisotropic elasto-plasticity coupled to anisotropic damage: Kirchhoff stress $\boldsymbol{\tau}^{\sharp}$ and modified Mandel stress $[\hat{\mathbf{M}}^{\sharp}_{\mathrm{d}\,[\bar{v}^{\sharp}]^{\mathrm{t}}}]^{\mathrm{t}}$.

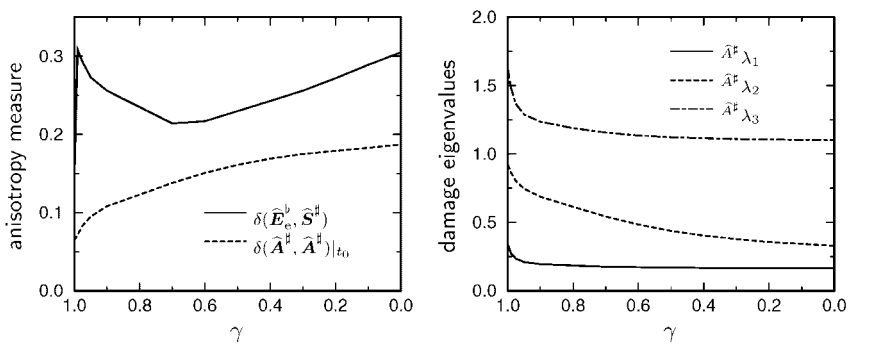

Figure 20. Simple shear, anisotropic elasto-plasticity coupled to anisotropic damage: Anisotropy measure $\delta(\hat{\mathbf{E}}^{\flat}_{\mathrm{e}}, \hat{\mathbf{S}}^{\sharp})$, $\delta(\hat{\mathbf{A}}^{\sharp}, \hat{\mathbf{A}}^{\sharp}|_{t_0})$ and eigenvalues of the damage metric ${}^{\hat{A}^{\sharp}}\lambda_{1,2,3}$.

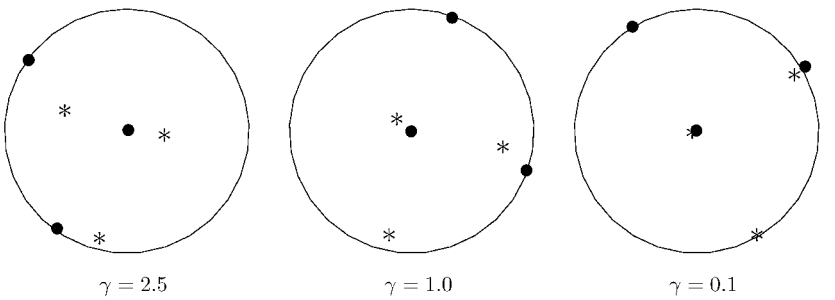

Figure 21. Simple shear, anisotropic elasto-plasticity coupled to anisotropic damage: Stereographic projection of strain ($\hat{\mathbf{E}}_e^{\flat} : \bullet$) and stress ($\hat{\mathbf{S}}^{\sharp} : *$).

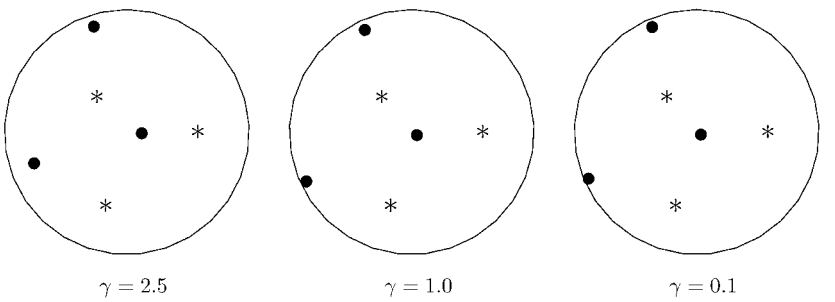

Figure 22. Simple shear, anisotropic elasto-plasticity coupled to anisotropic damage: Stereographic projection of the actual damage metric ($\hat{\mathbf{A}}^{\sharp} : \bullet$) and the initial damage metric ($\hat{\mathbf{A}}^{\sharp}|_{t_0} : *$).

7.1.4. Numerical aspects. As mentioned in Section 6, we applied a regula-falsi-type algorithm for the iteration for the Lagrange multiplier and Newton's method based on approximated Jacobians for the damage and plastic contributions and the exact Jacobian for the hardening part. Concerning the scalar-valued iteration scheme for the Lagrange multiplier, one has to make a choice for two initial values in order to start the computation. The trial guess zero is obvious but the second value affects the convergence of the iteration. Table I highlights this influence within the setting of anisotropic elasto-plasticity coupled to anisotropic damage evolution for the rather large load step $\gamma \in [0, 0.5]$ whereby $\|\mathbf{R}\|$ abbreviates the sum $\|{}^{\text{dam}}\hat{\mathbf{R}}^{\sharp}\| + \|{}^{\text{pla}}\mathbf{R}^{\sharp}\|$.

Moreover, the convergence of the Newton algorithm inside each regula-falsi step is crucially affected by the incorporated perturbation parameter ε for the numerically approximated Jacobians, compare Appendix A. Within the above examples, the chosen machine precision corresponds to a storeup of 16 digits. The influence of the perturbation parameter is given in Table II within the load step $\gamma \in [0, 0.5]$.

7.2. Stamping of a sheet

Within the subsequent finite element setting we account for anisotropic elasto-plasticity coupled to anisotropic damage evolution whereby the chosen set of material parameters is identical

Table I. Influence of different initial values for $\Delta\lambda_1$ on the convergence of the regula-falsi-type iteration for the Lagrange multiplier within the load step $\gamma \in [0, 0.5]$.

	$\Delta\lambda_1$	${}^{\text{yie}}\Phi^{\text{p}}$	$\Delta\lambda_1$	${}^{\text{yie}}\Phi^{\text{p}}$	$\Delta\lambda_1$	${}^{\text{yie}}\Phi^{\text{p}}$
No.	0.000 E − 16	2.068 E + 08	0.000 E − 16	2.068 E + 08	0.000 E − 16	2.068 E + 08
1	1.000 E − 06	1.018 E + 08	1.000 E − 05	2.803 E + 07	1.000 E − 04	1.325 E + 06
2	1.969 E − 06	7.710 E + 07	1.156 E − 05	2.482 E + 07	1.010 E − 04	1.301 E + 06
3	4.995 E − 06	4.640 E + 07	2.369 E − 05	1.246 E + 07	1.370 E − 04	3.621 E + 05
4	9.569 E − 06	2.905 E + 07	3.591 E − 05	7.704 E + 06	1.500 E − 04	1.282 E + 05
5	1.722 E − 05	1.726 E + 07	5.570 E − 05	4.217 E + 06	1.580 E − 04	1.955 E + 04
6	4.454 E − 05	1.017 E + 07	7.963 E − 05	2.259 E + 06	1.590 E − 04	1.260 E + 03
7	6.607 E − 05	5.821 E + 06	1.070 E − 04	1.079 E + 06	1.600 E − 04	1.335 E + 01
8	9.232 E − 05	3.198 E + 06	1.330 E − 04	4.418 E + 05	1.600 E − 04	9.230 E − 03
9	1.200 E − 04	1.628 E + 06	1.500 E − 04	1.351 E + 05	1.600 E − 04	1.752 E − 03
10	1.420 E − 04	7.330 E + 05	1.580 E − 04	2.416 E + 04	1.600 E − 04	4.346 E − 07
11	1.550 E − 04	2.679 E + 05	1.590 E − 04	1.631 E + 03		
12	1.590 E − 04	6.663 E + 04	1.600 E − 04	2.128 E + 01		
13	1.600 E − 04	8.115 E + 03	1.600 E − 04	1.902 E − 02		
14	1.600 E − 04	2.836 E + 02	1.600 E − 04	3.610 E − 03		
15	1.600 E − 04	1.255 E + 00	1.600 E − 04	1.141 E − 06		
16	1.600 E − 04	8.920 E − 04	1.600 E − 04	1.711 E − 09		
17	1.600 E − 04	1.690 E − 04				
18	1.600 E − 04	1.202 E − 08				

Table II. Influence of different perturbation factors ε on the convergence of the local Newton iteration within the load step $\gamma \in [0, 0.5]$ for $\Delta\lambda_1 = 10^{-4}$.

	$\|\mathbf{R}\|$ for $\varepsilon = 10^{-12}$		$\|\mathbf{R}\|$ for $\varepsilon = 10^{-8}$		$\|\mathbf{R}\|$ for $\varepsilon = 10^{-4}$	
No.	step 1	step 2	step 1	step 2	step 1	step 2
1	2.970 E + 01	3.264 E − 06	2.995 E + 01	3.451 E − 06	3.001 E + 01	9.142 E − 06
2	7.390 E + 01	2.570 E − 09	7.397 E + 01	1.584 E − 11	7.448 E + 01	1.522 E − 08
3	9.324 E + 00		9.383 E + 00		9.366 E + 00	
4	7.997 E − 01		6.915 E − 01		6.663 E − 01	
5	1.296 E − 01		1.217 E − 01		1.191 E − 01	
6	3.985 E − 03		3.525 E − 03		3.360 E − 03	
7	4.920 E − 06		4.418 E − 06		5.030 E − 06	
8	1.405 E − 09		1.889 E − 12		1.771 E − 09	

to that in Section 7.1.3 but $\delta_2 = 10$. The considered specimen consists of a plate-like structure of dimensions $10 \times 10 \times 0.5$ and a rigid square block with a cross-sectional area 2.5×2.5, see Figure 23. The discretization of the plate is performed by $16 \times 16 \times 8$ enhanced eight node bricks, Q1E9, as advocated by Simo and Armero [36]. Boundary conditions and the applied loading are given in Figure 24.

A typical necking behaviour is indicated by the load-displacement curve in Figure 25. Furthermore, the subsequent plots refer to a deformation $\|\mathbf{u}\| = 1.46$ which is almost triple

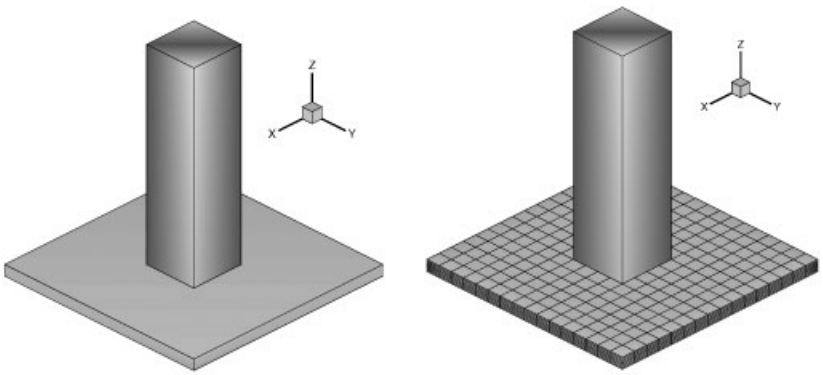

Figure 23. Anisotropic elasto-plasticity coupled to anisotropic damage evolution: Geometry and discretization of the specimen.

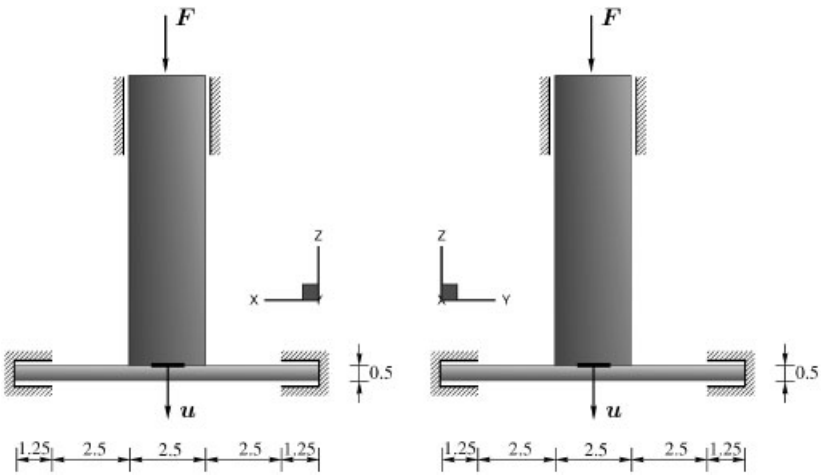

Figure 24. Anisotropic elasto-plasticity coupled to anisotropic damage evolution: Boundary conditions and loading of the specimen.

of the plate thickness. Figure 26 monitors the distribution of the deviatoric norm of the Kirchhoff stress $\| {}^{\mathrm{dev}}\boldsymbol{\tau}^{\sharp} \|$. In addition, one quarter of the body is zoomed. Even though geometry, boundary conditions and loading imply certain symmetries, the response of the specimen is completely non-symmetric which is due to the incorporated anisotropies. Apparently, the property of the contribution of the deviatoric norm of the modified Mandel stress $\| {}^{\mathrm{dev}}[\hat{\mathbf{M}}^{\natural}{}_{\mathrm{d}\,[\bar{v}^{\natural}]^{\natural}}]^{t} \|$ is different from those of the Kirchhoff stress, see Figure 27. The smallest eigenvalue of the damage metric tensor is visualized in Figure 28. Please note that ${}^{\hat{A}^{\sharp}}\lambda_1$ boils down from 1.00 to 0.55 which underlines a high degree of damage evolution. A typical indicator for anisotropy is the anisotropy measure $\delta(\hat{\mathbf{E}}_{\mathrm{e}}^{\flat}, \hat{\mathbf{S}}^{\sharp})$ as highlighted in Figure 29.

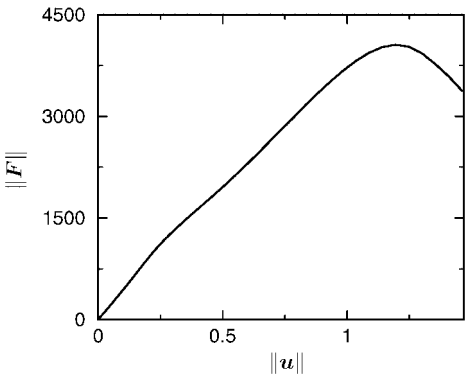

Figure 25. Anisotropic elasto-plasticity coupled to anisotropic damage evolution: Load-displacement curve.

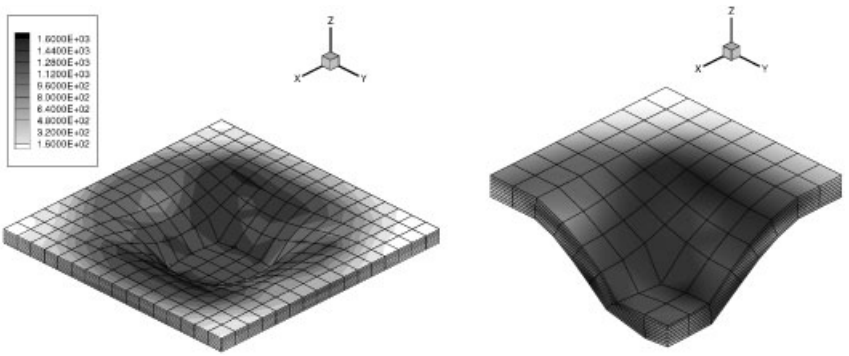

Figure 26. Anisotropic elasto-plasticity coupled to anisotropic damage evolution: Deviatoric norm of the Kirchhoff stress $\| {}^{\mathrm{dev}}\boldsymbol{\tau}^{\sharp} \|$.

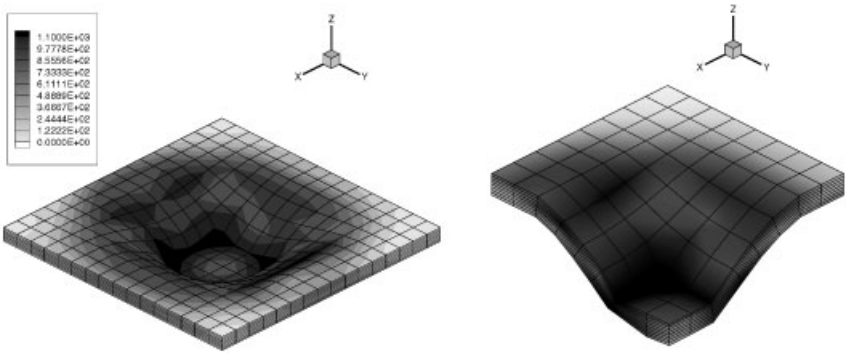

Figure 27. Anisotropic elasto-plasticity coupled to anisotropic damage evolution: Deviatoric norm of the modified Mandel stress $\| {}^{\mathrm{dev}}[\hat{\mathbf{M}}^{\sharp}_{\mathrm{d}\,[\bar{v}^{\alpha}]^{\mathrm{t}}}]^{\mathrm{t}} \|$.

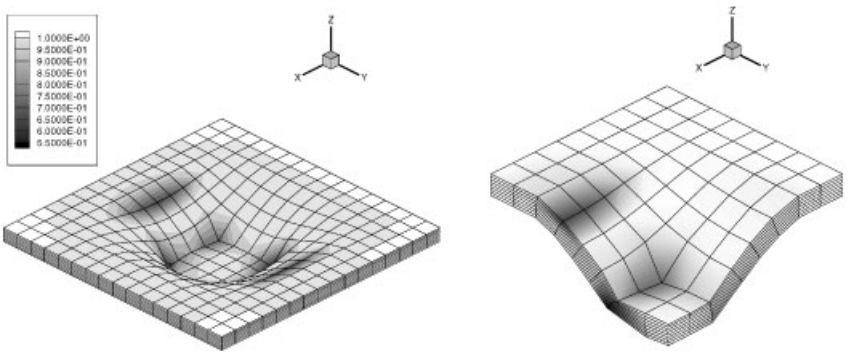

Figure 28. Anisotropic elasto-plasticity coupled to anisotropic damage evolution: Smallest damage eigenvalue ${}^{\hat{A}^\sharp}\lambda_1$.

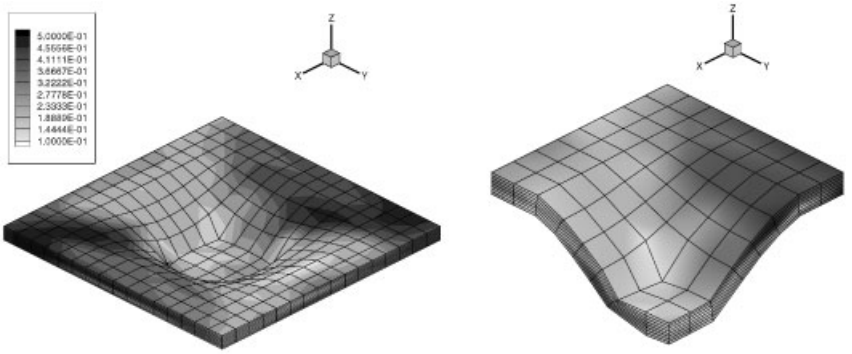

Figure 29. Anisotropic elasto-plasticity coupled to anisotropic damage evolution: Anisotropy measure $\delta(\hat{\mathbf{E}}_e^\flat, \hat{\mathbf{S}}^\sharp)$.

Moreover, the evolution of the principal axes of the damage metric is represented via the non-vanishing scalar $\delta(\hat{\mathbf{A}}^\sharp, \hat{\mathbf{A}}^\sharp|_{t_0})$ which allows interpretation as representing deformation induced anisotropy, see Figure 30. Finally the contributions of the hardening variable κ are monitored in Figure 31.

7.2.1. Numerical aspects. As previously mentioned, we numerically approximated the algorithmic tangent operator within the finite element setting, compare Appendix A. In this context, Table III monitors the dependence of the global convergence, $\|\mathbf{R}\|$, of the finite element scheme on the perturbation factor ε, similar to Section 7.1.4. Thereby we choose one load step that results from $\|\mathbf{u}\| = 0$ in $\|\mathbf{u}\| = 0.34$ and ${}^{\hat{A}^\sharp}\lambda_1 \in [1, 0.98]$ whereby the computations have been performed with the arc-length method. Recall that the applied machine precision corresponds to 16 decimal precisions.

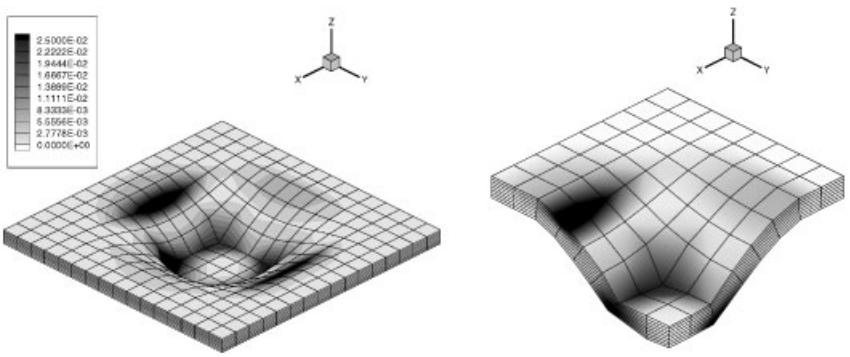

Figure 30. Anisotropic elasto-plasticity coupled to anisotropic damage evolution: Anisotropy measure $\delta(\hat{\mathbf{A}}^{\sharp}, \hat{\mathbf{A}}^{\sharp}|_{t_0})$.

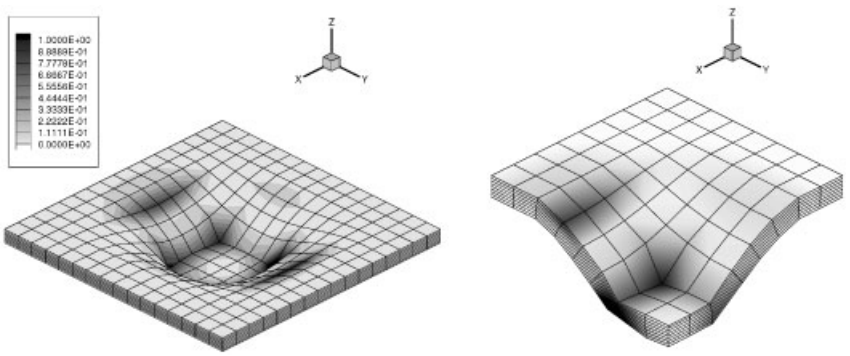

Figure 31. Anisotropic elasto-plasticity coupled to anisotropic damage evolution: Hardening variable κ.

Table III. Influence of different perturbation factors ε on the convergence of the global Newton iteration within the load step $\|\mathbf{u}\| \in [0, 0.34]$.

No.	$\varepsilon = 10^{-12}$ $\|\mathbf{R}\|$	$\varepsilon = 10^{-8}$ $\|\mathbf{R}\|$	$\varepsilon = 10^{-4}$ $\|\mathbf{R}\|$
1	2.6998 E + 03	2.6983 E + 03	2.6985 E + 03
2	6.8412 E + 02	6.7962 E + 02	6.8185 E + 02
3	5.9166 E + 01	5.1878 E + 01	5.1816 E + 01
4	2.4510 E + 00	1.0577 E + 00	1.0275 E + 00
5	1.4148 E − 01	2.0344 E − 02	2.0650 E − 02
6	1.2744 E − 02	8.3972 E − 07	2.4782 E − 04
7	7.6180 E − 04	2.7513 E − 09	3.2112 E − 05
8	4.7580 E − 05		4.5746 E − 06
9	5.2422 E − 06		6.5566 E − 07
10	1.1622 E − 06		9.4023 E − 08
11	1.3666 E − 07		1.3699 E − 08
12	1.8831 E − 08		

8. SUMMARY

The main goal of this contribution was the development of a framework for geometrically non-linear, anisotropic inelasticity with special emphasis on continuum damage coupled to plasticity. As the key idea, fictitious isotropic configurations have been introduced which are determined by fictitious linear tangent maps. Thus, we practically dealt with a reduced representation of orthotropy which is, nevertheless, of crucial importance for engineering applications.

The corresponding Finger-type tensor, in terms of a fictitious linear tangent map, was used as a damage metric which allowed to incorporate initial anisotropy as well as deformation induced anisotropy. Conceptually speaking, the applied covariance relation corresponds to the postulate of strain energy equivalence.

Then, for the coupling to plasticity, another fictitious configuration for the yield function has been introduced. Thereby, a specific kinematical assumption defines a stress tensor of Mandel-type which enters the yield function with respect to the intermediate configuration of multiplicative elasto-plasticity. This particular stress tensor accounts, in view of the plasticity framework, for anisotropy and degradation.

Within the outline of the applied numerical setting, the integration of the obtained evolution equations has been highlighted in detail whereby simple Euler backward and exponential schemes have been adopted. Summarizing, it turns out that the considered anisotropic framework results in a manageable numerical setting which is a main advantage of the proposed formulation. Concerning future research, the incorporation of an appropriate regularization technique will be of main importance.

In conclusion, this contribution aims at the clarification of how to formulate and to computationally treat anisotropic second-order continuum damage coupled to plasticity within a geometrically non-linear setting in a kinematically and thermodynamically consistent way.

APPENDIX A: APPROXIMATION OF JACOBIANS

For a general outline on approximation schemes for Jacobians, typically within a Newton iteration, we refer to Denis and Schnabel Reference [37]. This technique has been applied to a finite element setting under large, inelastic deformations by Miehe [38]. Recently, Pérez-Foguet *et al.* [39, 40] discussed this method within small strain, inelastic finite element applications and placed special emphasis on—what we call—the local and global iteration. Here, we adopt the outline given by Miehe [38]—on the local and global level—and end up with the algorithm highlighted in Table A1. Thereby, we have chosen an Eulerian setting for the algorithmic tangent operator within a finite element setting and $\boldsymbol{\gamma}^{\flat}_{(k,l)}$, $\boldsymbol{\gamma}^{\sharp(k)}$, $\hat{\boldsymbol{\Gamma}}^{\flat}_{(l)}$, $\hat{\boldsymbol{\Gamma}}^{\sharp(k,l)}$ denote admissible base vectors in $\mathscr{B}_t$ and $\mathscr{B}_{\mathrm{p}}$, respectively, with $i,j,(k),(l)=1,2,3$. The numerical computation of the Jacobians ${}^{\mathrm{dam}}\hat{\mathbf{J}}^{\sharp}_{\mathbf{F}^{\sharp}_{\mathrm{e}}}$ and ${}^{\mathrm{pla}}\mathbf{J}^{\sharp}_{\hat{\mathbf{A}}^{\sharp}}$ is similar to the outline given in Table A1 and the exact format of ${}^{\mathrm{har}}J_{\kappa}$ is obvious.

In order to underline that the numerical approximation of the Jacobians is appropriate for the presented framework, we give an example of the exact, analytical evaluation of one single fourth order contribution. Thus, the derivation of the 'simplest' Jacobian ${}^{\mathrm{dam}}\hat{\mathbf{J}}^{\sharp}_{\hat{\mathbf{A}}^{\sharp}}$ is highlighted.

Table A1. Numerical approximation of Jacobians ($\varepsilon_{1,2,3} \ll 1$).

Numerical derivatives wrt $\hat{\mathbf{A}}^{\sharp}$

$$
\begin{aligned}
{}^{n+1}\hat{\mathbf{A}}^{(kl)}_{\varepsilon_1} &= {}^{n+1}\hat{\mathbf{A}}^{\sharp} + \varepsilon_1 \hat{\mathbf{\Gamma}}^{\sharp\,(k)} \otimes \hat{\mathbf{\Gamma}}^{\sharp\,(l)} \\
{}^{\mathrm{dam}}\hat{\mathbf{R}}^{(kl)}_{\varepsilon_1} &= {}^{\mathrm{dam}}\hat{\mathbf{R}}\,({}^{n+1}\hat{\mathbf{A}}^{(kl)}_{\varepsilon_1}, \ldots) \\
{}^{\mathrm{dam}}\hat{J}^{ij}_{\hat{A}^{\sharp}\,(kl)\,\varepsilon_1} &= [{}^{\mathrm{dam}}\hat{R}^{ij(kl)}_{\varepsilon_1} - {}^{\mathrm{dam}}\hat{R}^{ij}]/\varepsilon_1
\end{aligned}
$$

Numerical derivatives wrt $\mathbf{F}^{\natural}_{\mathrm{e}}$

$$
\begin{aligned}
{}^{n+1}\mathbf{F}^{(k)}_{\mathrm{e}\,\varepsilon_2\,(l)} &= {}^{n+1}\mathbf{F}^{\natural}_{\mathrm{e}} + \varepsilon_2 \boldsymbol{\gamma}^{\sharp\,(k)} \otimes \hat{\mathbf{\Gamma}}^{\flat}_{(l)} \\
{}^{\mathrm{pla}}\mathbf{R}^{(k)}_{\varepsilon_2\,(l)} &= {}^{\mathrm{pla}}\mathbf{R}({}^{n+1}\mathbf{F}^{(k)}_{\mathrm{e}\,\varepsilon_2\,(l)}, \ldots) \\
{}^{\mathrm{pla}}J^{i\,(l)}_{F^{\natural}_{\mathrm{e}}j(k)\varepsilon_2} &= [{}^{\mathrm{pla}}R^{i\,(k)}_{\varepsilon_2 j\,(l)} - {}^{\mathrm{pla}}R^{i}_{j}]/\varepsilon_2
\end{aligned}
$$

Algorithmic tangent operator

$$
\begin{aligned}
{}^{n+1}\mathbf{F}_{\varepsilon_3\,(kl)} &= {}^{n+1}\mathbf{F}^{\natural} + \frac{\varepsilon_3}{2}[[\mathbf{g}^{\sharp} \cdot \boldsymbol{\gamma}^{\flat}_{(k)}] \otimes [\boldsymbol{\gamma}^{\flat}_{(l)} \cdot \mathbf{F}^{\natural}] + [\mathbf{g}^{\sharp} \cdot \boldsymbol{\gamma}^{\flat}_{(l)}] \otimes [\boldsymbol{\gamma}^{\flat}_{(k)} \cdot \mathbf{F}^{\natural}]] \\
{}^{n+1}\boldsymbol{\tau}_{\varepsilon_3\,(kl)} &= {}^{n+1}\boldsymbol{\tau}({}^{n+1}\mathbf{F}_{\varepsilon_3\,(kl)}, \ldots) \\
{}^{\mathrm{alg}}e^{ij(kl)}_{\varepsilon_3} &= [\tau^{ij}_{\varepsilon_3\,(kl)} - \tau^{ij}]/\varepsilon_3 - [g^{ik}\tau^{jl} + g^{il}\tau^{jk} + \tau^{ik}g^{jl} + \tau^{il}g^{jk}]/2
\end{aligned}
$$

In the case of quasi isotropic damage evolution, we obtain

$$
\begin{aligned}
{}^{\mathrm{dam}}\hat{\mathbf{J}}^{\natural}_{\hat{\mathbf{A}}^{\sharp}} = {} & [1 - \Delta\lambda\delta_1\, {}^{n+1}\hat{\mathbf{Z}}^{\flat} : {}^{n+1}\hat{\mathbf{A}}^{\sharp}]\; {}^{\mathrm{sym}}\hat{\mathbf{G}}^{\natural} \\
& - \Delta\lambda\delta_1\, {}^{n+1}\hat{\mathbf{A}}^{\sharp} \otimes [{}^{n+1}\hat{\mathbf{Z}}^{\flat} - {}^{n+1}\hat{\mathbf{A}}^{\sharp} : \partial^2_{{}^{n+1}\hat{\mathbf{A}}^{\sharp} \otimes {}^{n+1}\hat{\mathbf{A}}^{\sharp}} \psi^{\mathrm{p}}_0]
\end{aligned}
\tag{A1}
$$

and anisotropic damage results in

$$
\begin{aligned}
{}^{\mathrm{dam}}\hat{\mathbf{J}}^{\natural}_{\hat{\mathbf{A}}^{\sharp}} = {} & {}^{\mathrm{sym}^{\sharp}}\hat{\mathbf{G}}^{\natural} + \Delta\lambda\delta_2[{}^{n+1}\hat{\mathbf{A}}^{\sharp} \bar{\otimes} {}^{n+1}\hat{\mathbf{A}}^{\sharp}] : \partial^2_{{}^{n+1}\hat{\mathbf{A}}^{\sharp} \otimes {}^{n+1}\hat{\mathbf{A}}^{\sharp}} \psi^{\mathrm{p}}_0 \\
& - \Delta\lambda\delta_1 [\hat{\mathbf{G}}^{\natural} \bar{\otimes} [{}^{n+1}\hat{\mathbf{A}}^{\sharp} \cdot {}^{n+1}\hat{\mathbf{Z}}^{\flat}]\hat{\mathbf{G}}^{\natural} \underline{\otimes} [{}^{n+1}\hat{\mathbf{A}}^{\sharp} \cdot {}^{n+1}\hat{\mathbf{Z}}^{\flat}]]^{\mathrm{SYM}}
\end{aligned}
\tag{A2}
$$

with

$$
{}^{\mathrm{sym}^{\sharp}}\hat{\mathbf{G}}^{\natural} = \tfrac{1}{2}[\hat{\mathbf{G}}^{\natural} \bar{\otimes} \hat{\mathbf{G}}^{\natural} + \hat{\mathbf{G}}^{\natural} \underline{\otimes} \hat{\mathbf{G}}^{\natural}] \tag{A3}
$$

whereby the non-standard dyadic products read (with respect to a Cartesian frame)

$$
[\bullet]_{ij} \bar{\otimes} [\circ]_{kl} = [\bullet]_{ik}[\circ]_{jl}, \quad [\bullet]_{ij} \underline{\otimes} [\circ]_{kl} = [\bullet]_{il}[\circ]_{jk} \tag{A4}
$$

and the major symmetry operation is defined as $2[\bullet]^{\mathrm{SYM}}_{ijkl} = [\bullet]_{ijkl} + [\bullet]_{klij}$, respectively. Moreover, the evaluation of the incorporated Hessian yields after some straightforward

computations

$$
\begin{aligned}
\partial^2_{{}^{n+1}\hat{\mathbf{A}}^\sharp \otimes {}^{n+1}\hat{\mathbf{A}}^\sharp} \psi_0^{\mathrm{p}} = {} & \partial^2_{\hat{E}^\flat \hat{A}^\sharp I_1 \hat{E}^\flat \hat{A}^\sharp I_1} \psi_0^{\mathrm{p}} \hat{\mathbf{E}}^\flat \otimes \hat{\mathbf{E}}^\flat \\
& + 4 \partial^2_{\hat{E}^\flat \hat{A}^\sharp I_2 \hat{E}^\flat \hat{A}^\sharp I_2} \psi_0^{\mathrm{p}} [\hat{\mathbf{E}}^\flat \cdot \hat{\mathbf{A}}^\sharp \cdot \hat{\mathbf{E}}^\flat] \otimes [\hat{\mathbf{E}}^\flat \cdot \hat{\mathbf{A}}^\sharp \cdot \hat{\mathbf{E}}^\flat] \\
& + 9 \partial^2_{\hat{E}^\flat \hat{A}^\sharp I_3 \hat{E}^\flat \hat{A}^\sharp I_3} \psi_0^{\mathrm{p}} [\hat{\mathbf{E}}^\flat \cdot \hat{\mathbf{A}}^\sharp \cdot \hat{\mathbf{E}}^\flat \cdot \hat{\mathbf{A}}^\sharp \cdot \hat{\mathbf{E}}^\flat] \otimes [\hat{\mathbf{E}}^\flat \cdot \hat{\mathbf{A}}^\sharp \cdot \hat{\mathbf{E}}^\flat \cdot \hat{\mathbf{A}}^\sharp \cdot \hat{\mathbf{E}}^\flat] \\
& + 4 \partial^2_{\hat{E}^\flat \hat{A}^\sharp I_1 \hat{E}^\flat \hat{A}^\sharp I_2} \psi_0^{\mathrm{p}} [\hat{\mathbf{E}}^\flat \otimes [\hat{\mathbf{E}}^\flat \cdot \hat{\mathbf{A}}^\sharp \cdot \hat{\mathbf{E}}^\flat]]^{\mathrm{SYM}} \\
& + 12 \partial^2_{\hat{E}^\flat \hat{A}^\sharp I_2 \hat{E}^\flat \hat{A}^\sharp I_3} \psi_0^{\mathrm{p}} [[\hat{\mathbf{E}}^\flat \cdot \hat{\mathbf{A}}^\sharp \cdot \hat{\mathbf{E}}^\flat] \otimes [\hat{\mathbf{E}}^\flat \cdot \hat{\mathbf{A}}^\sharp \cdot \hat{\mathbf{E}}^\flat \cdot \hat{\mathbf{A}}^\sharp \cdot \hat{\mathbf{E}}^\flat]]^{\mathrm{SYM}} \\
& + 6 \partial^2_{\hat{E}^\flat \hat{A}^\sharp I_1 \hat{E}^\flat \hat{A}^\sharp I_3} \psi_0^{\mathrm{p}} [\hat{\mathbf{E}}^\flat \otimes [\hat{\mathbf{E}}^\flat \cdot \hat{\mathbf{A}}^\sharp \cdot \hat{\mathbf{E}}^\flat \cdot \hat{\mathbf{A}}^\sharp \cdot \hat{\mathbf{E}}^\flat]]^{\mathrm{SYM}} \\
& + \partial_{\hat{E}^\flat \hat{A}^\sharp I_2} \psi_0^{\mathrm{p}} [\hat{\mathbf{E}}^\flat \bar{\otimes} \hat{\mathbf{E}}^\flat + \mathbf{E}^\sharp \underline{\otimes} \hat{\mathbf{E}}^\flat] \\
& + 3 \partial_{\hat{E}^\flat \hat{A}^\sharp I_3} \psi_0^{\mathrm{p}} [\hat{\mathbf{E}}^\flat \bar{\otimes} [\hat{\mathbf{E}}^\flat \cdot \hat{\mathbf{A}}^\sharp \cdot \hat{\mathbf{E}}^\flat] + \hat{\mathbf{E}}^\flat \underline{\otimes} [\hat{\mathbf{E}}^\flat \cdot \hat{\mathbf{A}}^\sharp \cdot \hat{\mathbf{E}}^\flat]]^{\mathrm{SYM}}
\end{aligned} \tag{A5}
$$

For the chosen prototype model, the Neo–Hookian part ${}^{\mathrm{dam}}\psi_0^{\mathrm{p}}$ is highly non-linear in $\hat{\mathbf{E}}^\flat$ and $\hat{\mathbf{A}}^\sharp$. Thus is turns out that the numerical approximation of the Jacobian in Equations (A1) and (A2), and apparently the approximation of the other fourth order Jacobians in Equation (67) as well, is not immoderately expensive compared to the exact computation.

ACKNOWLEDGEMENTS

Financial support from the Stiftung Rheinland-Pfalz für Innovation under research grant 8312-38 62 61/378 is gratefully acknowledged.

REFERENCES

1. Leckie FA, Onat ET. Tensorial nature of damage measuring internal variables. In *Physical Non-Linearities in Structural Analysis*, Hult J, Lemaitre J (eds), IUTAM Symposium Senlis/France 1980. Springer: Berlin, 1981; 140–155.
2. Betten J. Representation of constitutive equations in creep mechanics of isotropic and anisotropic materials. In *Creep in Structures*, Ponter ARS, Hayhurst DR (eds), IUTAM Symposium Leicester/UK 1980. Springer: Berlin, 1981; 179–201.
3. Murakami S. Mechanical modeling of material damage. *Journal of Applied Mechanics* (ASME) 1988; **55**: 280–286.
4. Kattan PI, Voyiadjis GZ. A coupled theory of damage mechanics and finite strain elasto-plasticity—I. Damage and elastic deformations. *International Journal of Engineering Science* 1990; **28**(5):421–435.
5. Steinmann P, Carol I. A framework for geometrically nonlinear continuum damage mechanics. *International Journal of Engineering Science* 1998; **36**:1793–1814.
6. Hansen NR. Schreyer HL. A thermodynamically consistent framework for theories of elastoplasticity coupled with damage. *International Journal of Solids and Structures* 1994; **31**(3):359–389.
7. Voyiadjis GZ, Park T. The kinematics of damage for finite-strain elasto-plastic solids. *International Journal of Engineering Science* 1999; **37**:803–830.
8. Menzel A, Ekh M, Steinmann P, Runesson K. Anisotropic damage coupled to plasticity: Modelling based on the effective configuration concept. *International Journal for Numerical Methods in Engineering* 2002; **54**(10):1409–1430.

9. Oller S, Botello S, Miquel J, Oñate E. An anisotropic elastoplastic model based on an isotropic formulation. *Engineering Computations* 1995; **12**:245–262.
10. Lubliner J. *Plasticity Theory*. Macmillan: New York, 1990.
11. Haupt P. Continuum mechanics and theory of materials. In *Advanced Texts in Physics*. Springer: Berlin, 2000.
12. Naghdi PM. A critical review of the state of finite plasticity. *Zeitschrift fur Angewandte Mathematik und Physik* 1990; **41**:315–394.
13. Brünig M. A framework for large strain elastic-plastic damage mechanics based on metric transformation tensors. *International Journal of Engineering Science* 2001; **39**:1033–1056.
14. Lemaitre J, Chaboche J-L. *Mechanics of Solid Materials*. 2nd paperback edn. Cambridge, 1998.
15. Green AE, Zerna W. *Theoretical Elasticity*. Dover: New York, 1992.
16. Lodge AS. *Body Tensor Fields in Continuum Mechanics* (*With Application to Polymer Rheology*). Academic Press: New York, 1974.
17. Marsden JE, Hughes TJR. *Mathematical Foundations of Elasticity*. Dover: New York, 1994.
18. Menzel A, Steinmann P. On the comparison of two strategies to formulate orthotropic hyperelasticity. *Journal of Elasticity* 2001; **62**:171–201.
19. Svendsen B. On the modeling of anisotropic elastic and inelastic material behaviour at large deformation. *International Journal of Solids and Structures* 2001; **38**(52):9579–9599.
20. Sidoroff F. Description of anisotropic damage application to elasticity. In *Physical Non-Linearities in Structural Analysis*, Hult J, Lemaitre J (eds), IUTAM Symposium Senlis/France, 27.–30.05.1980. Springer: Berlin, 1981; 237–244.
21. Spencer AJM. Constitutive theory of strongly anisotropic solids. In *Continuum Theory of the Mechanics of Fibre-Reinforced Composites*, Spencer AJM (ed.), CISM Courses and Lectures, vol. 282. Springer: Berlin, 1984.
22. Halphen B, Nguyen QS. Sur les matériaux standards généralisés. *Journal de Mécanique* 1975; **14**:39–62.
23. Maugin GA. The thermodynamics of nonlinear irreversible behaviors, *World Scientific Series on Nonlinear Science*: *Series A*, vol. 27. World Scientific: Singapore, 1999.
24. Antman SS. Nonlinear problems of elasticity. In *Applied Mathematical Sciences*, vol. 107. Springer: Berlin, 1995.
25. Maugin GA. Eshelby stress in elastoplasticity and ductile fracture. *International Journal of Plasticity* 1994; **10**(4):393–408.
26. Miehe C, Stein E. A canonical model of multiplicative elasto-plasticity: Formulation and aspects of the numerical implementation. *European Journal of Mechanics—A/Solids* 1992; **11**:25–43. Special issue.
27. Betten J. The classical plastic potential theory in comparison with the tensor function theory. *Engineering Fracture Mechanics* 1985; **21**(4):641–652.
28. Schreyer HL. Continuum damage based on elastic projection tensors. *International Journal of Damage Mechanics* 1995; **4**:171–195.
29. Menzel A, Steinmann P. A theoretical and computational setting for anisotropic continuum damage mechanics at large strains. *International Journal of Solids and Structures* 2001; **38**(52):9505–9523.
30. Steinmann P, Miehe C, Stein E. Comparison of different finite deformation inelastic damage models within multiplicative elastoplasticity for ductile materials. *Computational Mechanics* 1994; **13**:458–474.
31. Lämmer H, Tsakmakis C. Discussion of coupled elastoplasticity and damage constitutive equations for small and finite deformations. *International Journal of Plasticity* 2000; **16**:495–523.
32. Dafalias YF. Plastic spin: Necessity or redundancy? *International Journal of Plasticity* 1998; **14**(9):909–931.
33. Simo JC. Numerical analysis and simulation of plasticity. In *Numerical Methods for Solids* (*Part 3*), Ciarlet PG, Lions JL (eds), *Handbook of Numerical Analysis*, vol. VI. North-Holland, Amsterdam, 1998.
34. Weber G, Anand L. Finite deformation constitutive equations and a time integration procedure for isotropic, hyperelastic-viscoplastic solids. *Computer Methods in Applied Mechanics and Engineering* 1990; **79**:173–202.
35. de Souza Neto EA. The exact derivative of the exponential of an unsymmetric tensor. *Computer Methods in Applied Mechanics and Engineering* 2001; **190**:2377–2383.
36. Simo JC, Armero F. Geometrically non-linear enhanced strain mixed methods and the method of incompatible modes. *International Journal for Numerical Methods in Engineering* 1992; **33**:1413–1449.
37. Dennis Jr JE, Schnabel RB. Numerical methods for unconstrained optimization and nonlinear equations. In *Classics in Applied Mathematics*, vol. 16. SIAM: Philadelphia, 1996.
38. Miehe C. Numerical computation of algorithmic (consistent) tangent moduli in large-strain computational inelasticity. *Computer Methods in Applied Mechanics and Engineering* 1996;**134**:223–240.
39. Pérez-Foguet A, Rodriguez-Ferran A, Huerta A. Numerical differentiation for local and global tangent operators in computational plasticity. *Computer Methods in Applied Mechanics and Engineering* 2000; **189**:277–296.
40. Pérez-Foguet A, Rodriguez-Ferran A, Huerta A. Numerical differentiation for non-trivial consistent tangent matrices: An application to the MRS-Lade model. *International Journal for Numerical Methods in Engineering* 2000; **48**:159–184.

